HIGH REDSHIFT GALAXIES IN THE HUBBLE DEEP FIELD. COLOR SELECTION AND STAR FORMATION HISTORY TO z ∼ 4 [1]

Piero Madau, Henry C. Ferguson, Mark E. Dickinson
Space Telescope Science Institute, 3700 San Martin Drive, Baltimore MD 21218, USA
e-mail: madau@stsci.edu, ferguson@stsci.edu, med@stsci.edu

Mauro Giavalisco[2]
Carnegie Observatories, 813 Santa Barbara Street, Pasadena, Ca 91101-1292
e-mail: mauro@ociw.edu

Charles C. Steidel[3,4]
Palomar Observatory, California Institute of Technology, Mail Stop 105-24, Pasadena, CA 91125
e-mail: ccs@astro.caltech.edu

Andrew Fruchter
Space Telescope Science Institute, 3700 San Martin Drive, Baltimore MD 21218
e-mail: fruchter@stsci.edu

ABSTRACT

The Lyman decrement associated with the cumulative effect of H I in QSO absorption systems along the line of sight provides a distinctive feature for identifying galaxies at $z \gtrsim 2.5$. Color criteria, which are sensitive to the presence of a Lyman-continuum break superposed on an otherwise flat UV spectrum, have been shown, through Keck spectroscopy, to successfully identify a substantial population of star-forming galaxies at $3 \lesssim z \lesssim 3.5$ (Steidel et al. 1996a). Such objects have proven surprisingly elusive in field-galaxy redshift surveys; quantifying their surface density and morphology is crucial for determining how and when galaxies formed. The *Hubble Deep Field* (HDF) observations offer the opportunity to exploit the ubiquitous effect of intergalactic absorption and obtain useful statistical constraints on the redshift distribution of galaxies considerably fainter than current spectroscopic limits. We model the H I cosmic opacity as a function of redshift, including scattering in resonant lines of the Lyman series and Lyman-continuum absorption, and use stellar population synthesis models with a wide variety of ages, metallicities, dust contents, and redshifts, to derive color selection criteria that provide a robust separation between high redshift and low redshift galaxies. From the HDF images we construct a sample of star-forming galaxies at $2 \lesssim z \lesssim 4.5$. While none of the ~ 60 objects in the HDF having known Keck/LRIS spectroscopic redshifts in the range $0 \lesssim z \lesssim 1.4$ is found to contaminate our high-redshift sample, our color criteria are able to efficiently select the $2.6 \lesssim z \lesssim 3.2$ galaxies identified by Steidel et al. (1996b).

The ultraviolet (and blue) dropout technique opens up the possibility of investigating cosmic star and element formation in the early universe. We set a lower-limit to the ejection rate of heavy elements per unit comoving volume from Type II supernovae at $\langle z \rangle = 2.75$ of $\approx 3.6 \times 10^{-4} \, \mathrm{M_\odot \, yr^{-1} \, Mpc^{-3}}$ (for $q_0 = 0.5$ and $H_0 = 50 \, \mathrm{km \, s^{-1} \, Mpc^{-1}}$), which is 3 times higher than the local value, but still 4 times lower than the rate observed at $z \approx 1$. At $\langle z \rangle = 4$, our lower limit to the cosmic metal ejection rate is ≈ 3 times lower than the $\langle z \rangle = 2.75$ value. We discuss the implications of these results on models of galaxy formation, and on the chemical enrichment and ionization history of the intergalactic medium.

Subject headings: cosmology: observations – galaxies: evolution – intergalactic medium – quasars: absorption lines – ultraviolet: galaxies

---

1. INTRODUCTION

Much observing time has been devoted in the past few years to the problem of the detection of galaxies at high redshift, as it is anticipated that any knowledge of their early luminosity and color evolution will put constraints on the history of structure and metal formation. While it has become clear that blank-sky surveys for strong Lyα -emitting primeval galaxies are not particularly efficient (e.g., Pritchet & Hartwick 1990; Djorgovski & Thompson 1992), the method of obtaining multicolor broadband observations of the emitter's rest-frame UV stellar continuum has been successfully applied to detect galaxies at cosmological distances (Steidel et al. 1996a).

Ground-based observations have used color techniques which are sensitive to the presence of a Lyman-continuum break to identify or set limits on the number of high redshift galaxies (Steidel & Hamilton 1992, 1993). The signature of a distant, star-forming galaxy in such surveys is a very red $U-B$ color, combined with colors in longer-wavelength filters that are much bluer. The early work by Guhathakurta et al. (1990) showed that Lyman-break objects do not dominate the galaxy counts at faint apparent magnitudes. Assuming that young, star-forming galaxies have flat spectra longward of the Lyman-break, Steidel & Hamilton (1992, 1993), and Steidel, Pettini, & Hamilton (1995) have designed and used a custom set of broad-band filters to select high-z galaxies in the fields of distant QSOs. Recent deep spectroscopy with the W. M. Keck telescope has shown the high efficiency of such color-selection technique: Steidel et al. (1996a) have identified 17 Lyman-break star-forming galaxies with redshifts $3.0 \lesssim z \lesssim 3.5$, which are most likely the progenitors of the present-day bright spirals and ellipticals observed during the assembly of their cores (Giavalisco, Steidel, & Macchetto 1996).

With its high spatial resolution, the *Hubble Space Telescope* (HST) offers the opportunity to study the faint galaxy population in unprecedented detail. In particular, the images of the *Hubble Deep Field* (HDF), obtained with the Wide Field Planetary Camera (WFPC-2) during December 1995, represent the deepest optical imaging survey undertaken so far (Williams et al. 1996), reaching 5-σ limiting AB magnitudes of roughly 27.7, 28.6, 29.0, and 28.4 (for an aperture area of 0.2 square arcsec) in the F300W, F450W, F606W, and F814W bandpasses (the number corresponds to the central wavelength in nm), respectively. In this paper, we describe selection criteria for this filter system that can be used to identify a sample of likely precursors to present day galaxies at $z > 2$, with little contamination from low redshift galaxies. Our strategy is designed to exploit the effect of the increasing opacity of the intergalactic medium (IGM) at high redshifts, as indicated by the plethora of absorption lines seen in the spectra of background quasars: enough neutral hydrogen is known to be contained in the clumps of highly ionized gas which form the Lyα forest, and in the metal-line absorption systems associated with the halo regions of intervening bright galaxies, to significantly attenuate the UV flux from distant sources. We show that the cumulative effect of H I in QSO absorption systems along the line of sight provides a distinctive feature for identifying star-forming galaxies in the HDF. Although other spectral features, such as the 4000 and 912 Å breaks which characterize the integrated spectra of stellar populations, with the latter possibly enhanced by self-absorption from interstellar gas within the galaxy itself, may also be used as tracers of redshifts, the model predictions of their magnitude are sensitive to the unknown physical and evolutionary state of the galaxy, i.e., its star formation history, age, and H I distribution, and hence are subject to substantial uncertainties. By contrast, the "reddening" effect due to atomic processes in cosmological distributed QSO absorption systems is ubiquitous, quite strong for $z \gtrsim 2.5$, and can be reliably taken into account. Although stochastic in nature, r.m.s. fluctuations away from the mean opacity are bound to be modest in most situations, due to the broadband nature of the adopted filter set.

The technique to analyze the HDF images we develop in this paper is based on the theoretical study by Madau (1995) (see also Yoshii & Peterson 1994), and is an extension of the Lyman-break color criterion developed by Steidel & Hamilton (1992, 1993), and Steidel, Pettini, & Hamilton (1995). We extend this technique to the HDF filter system, and perform several experiments with simulated and real galaxy spectra to define effective selection criteria for high redshift galaxies, and identify possible sources of contamination

from low redshifts. By computing colors for an extremely wide range of model galaxy spectra, we are able to tune the criteria to provide what we believe are largely uncontaminated samples of star-forming galaxies in the redshift ranges $2 < z < 3.5$ and $3.5 < z < 4.5$, and use these samples to estimate the integrated star formation and metal ejection rates at those redshifts. We show how follow-up spectroscopy with Keck/LRIS by Steidel et al. (1996b), the Hawaii+Caltech group (Cohen et al. 1996), and the Berkeley HDF group (Moustakas, Zepf, & Davis 1996) supports the efficiency of our color selection techniques. Future work on high redshift galaxies in the HDF will investigate the luminosity function, study the morphologies, and compare the numbers and properties of high-z candidates to the predictions of a variety of galaxy-evolution models.

Throughout this paper, unless otherwise stated we shall adopt a flat cosmology with $q_0 = 0.5$ and $H_0 = 50 \, \mathrm{km \, s^{-1} \, Mpc^{-1}}$.

2. INTERGALACTIC ATTENUATION

In this section we will briefly review the theory of the propagation of UV radiation through a clumpy universe, following Madau (1995).

2.1. Basic Equations

Let $L(\nu_{\mathrm{em}})$ be the specific power emitted with frequency ν_{em} by a source at redshift z_{em}. The mean specific flux observed at Earth is

$$\langle f(\nu_{\mathrm{obs}}) \rangle = \frac{(1 + z_{\mathrm{em}}) L(\nu_{\mathrm{em}})}{4 \pi d_L^2} \langle e^{-\tau} \rangle, \tag{1}$$

where $\nu_{\mathrm{obs}} = \nu_{\mathrm{em}}/(1 + z_{\mathrm{em}})$, d_L is the luminosity distance to z_{em}, and the average transmission over all lines of sight is, assuming Poisson-distributed clouds,

$$\langle e^{-\tau} \rangle = \exp \left\{ \int_0^{z_{\mathrm{em}}} \int \frac{\partial^2 N}{\partial N_{\mathrm{HI}} \partial z} \left[1 - e^{-\tau_c} \right] dN_{\mathrm{HI}} dz \right\}. \tag{2}$$

Here, τ_c is the optical depth through an individual cloud at frequency $\nu = \nu_{\mathrm{obs}}(1 + z)$, and $(\partial^2 N / \partial N_{\mathrm{HI}} \partial z)$ is the redshift and column density distribution of absorbers along the path. An "effective" optical depth of a clumpy medium can be defined as $\tau_{\mathrm{eff}} = -\ln(\langle e^{-\tau} \rangle)$.

Along with resonant line scattering from Lyα, β, γ, and higher order members, we include photoelectric absorption from H I in the Lyα forest clouds and Lyman-limit systems along the line of sight. Since the bluest filter used for the HDF observations is centered at 3000 Å and has FWHM$\sim$ 800 Å, galaxies will only be subject to H I cosmological attenuation from material located at $z \gtrsim (2600/1216) - 1 = 1.1$.

2.2. Line Blanketing & Continuum Absorption

For $\lambda_\beta(1 + z_{\mathrm{em}}) < \lambda_{\mathrm{obs}} < \lambda_\alpha(1 + z_{\mathrm{em}})$, where $\lambda_\alpha = 1216$ Å and $\lambda_\beta = 1026$ Å, a galaxy's continuum intensity is attenuated by the combined blanketing effect of many Lyα forest absorption lines, with effective opacity

$$\tau_{\mathrm{eff}} = 0.0036 \left(\frac{\lambda_{\mathrm{obs}}}{\lambda_\alpha} \right)^{3.46}, \tag{3}$$

(Press, Rybicki, & Schneider 1993). Hence, line blanketing from Lyα alone will produce $\gtrsim 1$ mag of attenuation in the continuum spectrum shortward of 6000 Å of a galaxy at $z_{\mathrm{em}} \gtrsim 4$.

When $\lambda_{\mathrm{obs}} \leq \lambda_\beta(1 + z_{\mathrm{em}})$, a significant contribution to the blanketing opacity comes from the higher order lines of the Lyman series. A standard curve of growth analysis has been applied to numerically compute the attenuation expected from line blanketing of Lyβ, γ, δ plus 13 higher order members. In the

wavelength range $\lambda_{i+1}(1 + z_{\rm em}) < \lambda_{\rm obs} < \lambda_i(1 + z_{\rm em})$, the total optical depth can be written as the sum of the contributions from the $j \to 1$ transitions,

$$\tau_{\rm eff} = \sum_{j=2,i} A_j \left(\frac{\lambda_{\rm obs}}{\lambda_j}\right)^{3.46},$$ (4)

where $A_j = (1.7 \times 10^{-3}, 1.2 \times 10^{-3}, 9.3 \times 10^{-4})$, and $\lambda_j = (1026, 973, 950\,\text{Å})$ for Lyβ, γ, and δ, respectively. It is worth noting that heavy element absorbers make a negligible contribution to the blanketing optical depth at high redshifts, as this is dominated by those lines which lie at the transition between the linear and the flat part of the curve of growth, i.e., with $N_{\rm HI} \approx 10^{13.6}\,{\rm cm}^{-2}$ in the case of Lyα .

Continuum absorption by H I affects photons observed at $\lambda_{\rm obs} < \lambda_L(1 + z_{\rm em})$, where $\lambda_L = 912\,\text{Å}$ is the Lyman limit. An approximate (within 5%) integration of equation (2) yields for the effective photoelectric optical depth along the line of sight:

$$\tau_{eff} = 0.25x_c^3(x_{em}^{0.46} - x_c^{0.46}) + 9.4x_c^{1.5}(x_{em}^{0.18} - x_c^{0.18}) - 0.7x_c^3(x_c^{-1.32} - x_{em}^{-1.32}) - 0.023(x_{em}^{1.68} - x_c^{1.68}),$$ (5)

where $x_c = (\lambda_{\rm obs}/\lambda_L)$ for $\lambda_{\rm obs} > \lambda_L$, and $x_{em} = 1 + z_{em}$. The first term on the right-hand side represents the approximate contribution of Lyman-α clouds, the others are due to Lyman-limit systems. Absorbers with $N_{\rm HI} \sim 10^{17}\,{\rm cm}^{-2}$ dominate the cosmic continuum opacity.[5]

While our formula for the line blanketing optical depth is entirely consistent with the flux deficits D_A and D_B observed in the spectra of QSOs below their Lyα and Lyβ emission features (e.g., Schneider, Schmidt, & Gunn 1991), the derived continuum opacity is subject to significant uncertainties, as very limited information exist on optically thin absorbers with $10^{16} \lesssim N_{\rm HI} \lesssim 10^{17}\,{\rm cm}^{-2}$.

2.3. Cosmic Transmission

Figure 1a shows the characteristic staircase profile (cf Møller & Jakobsen 1990) of the mean cosmic transmission $\langle e^{-\tau} \rangle$ for a source at $z_{\rm em} = 3$, 4, and 5, as a function of observed wavelength. Also plotted are the response functions of the photometric system we shall adopt in our discussion. This consists of the four broad *HST* passbands F300W, F450W, F606W, and F814W (roughly $UBVI$). These filters efficiently cover most of the bandpass accessible to the *HST* WFPC-2.

It is clear that the observed broadband colors of cosmological distant objects will be strongly "reddened" by continuum absorption and blanketing of discrete absorption lines which move into and out of the color passbands with changing z. To be quantitative, we must take into account that the mean transmission observed is not $\langle e^{-\tau} \rangle$ but rather an average over the bandpass,

$$Q(z_{\rm em}) = \int e^{-\tau_{\rm eff}} T(\lambda) d\lambda,$$ (6)

where $T(\lambda)$ is the normalized transmittance of the relevant filter. In the following, we shall measure the mean integrated intergalactic attenuation in magnitudes, $\Delta m = -1.086 \ln Q$. Figure 1b shows ΔU_{300}, ΔB_{450}, ΔV_{606}, and ΔI_{814}, the observed magnitude increases at the corresponding bandpass due to intervening absorption, as a function of emission redshift in the redshift range $1.5 < z < 5$. [These increments must be added to the term $-1.086 \ln(1 + z_{\rm em})$ to get the standard K-correction for a flat emitted spectrum.]

We are now able to assess how intergalactic absorption will modify the intrinsic photometric properties of galaxies at high redshift. At $z_{\rm em} \approx 1.5$, Lyα line blanketing starts to cause a small apparent depression in the U_{300}-band continuum. As higher order lines of the Lyman series move into the bandpass, ΔU_{300}

---

[5] The He I contribution to the attenuation is negligible in the case of a QSO-dominated ionizing background, while He II absorption on the way must be included if $(1 + z_{\rm em}) > \lambda_{\rm obs}/228\text{Å}$ (e.g., Madau 1992).

increases rapidly until, at $z_{\rm em} = 2.3$, sources in the background appear, on average, ≈ 0.7 mag fainter in the ultraviolet. By $z_{\rm em} = 3$, Lyman-continuum absorption from forest clouds and Lyman-limit systems is so severe that $\Delta U_{300} \approx 2.8$ mag (of which ≈ 1.9 mag are due to Lyα clouds alone): galaxies will either appear very red in $U_{300} - B_{450}$ or will drop out of the F300W image altogether.[6] Similarly, the Lyα line progressively enters the F450W band beyond $z_{\rm em} \approx 2.7$. At $z_{\rm em} = 3.8$, line blanketing from the Lyman series produces $\Delta B_{450} \approx 1.2$ mag. By $z_{\rm em} = 4.4$, Lyman-continuum absorption contributes significantly to the total opacity, and ΔB_{450} exceeds 3.3 mag. The F606W bandpass is only weakly affected by intergalactic absorption for $z_{\rm em} \lesssim 4$. Hence, again, star-forming galaxies at $z_{\rm em} \sim 4$ will either appear very red in $B_{450} - V_{606}$ or will effectively be undetectable in the blue band. By $z_{\rm em} = 4.6$, line blanketing from the Lyman series produces $\Delta V_{606} \approx 1$ mag. As H I absorption does not affect the F814W passband for $z_{\rm em} \lesssim 5.7$, $\Delta I_{814} = 0$ in the redshift range of interest here.

Although Figure 1b refers to the average accumulated absorption only, r.m.s. fluctuations away from the mean transmission are predicted to be relatively small after integration over broad bandpasses (Press et al. 1993). For example, the observed B_{450}-band continuum of a galaxy at $z_{\rm em} \gtrsim 3$ is attenuated by the blanketing of more than 90 Lyα lines with $W > 0.3$Å along the light travel path. At these redshifts, excursions away from the average curve will be the largest in the F300W filter, due to the contribution to the photoelectric opacity by the rarer, optically thick Lyman-limit systems. Even in this case, however, with $dN/dz \approx 0.27(1 + z)^{1.55}$ absorbers per unit redshift with $N_{\rm HI} > 1.6 \times 10^{17}$ cm^{-2} (Storrie-Lombardi et al. 1994), as many as $\Delta N \sim 1.5$ Lyman-limit systems along a random path to $z_{\rm em} \gtrsim 2.7$ would be expected, on average, to photoelectrically absorb photons in the ultraviolet bandpass. As the probability of intersecting at least one metal system is large, $1 - e^{-\Delta N} \approx 80\%$, we expect only one out of five star-forming galaxies at $z > 2.7$ to be effectively detectable in the ultraviolet bandpass.

3. THE COLORS OF HIGH REDSHIFT GALAXIES

One of the major objectives of the HDF observations is to determine the morphology, spectral energy distribution, and number density of galaxies actively forming stars at high-z, the nature of which is crucial to our understanding of galaxy evolution. In this section we shall show how we can use intergalactic absorption to identify high redshift galaxies in broadband multicolor surveys. Colors can be more readily interpreted using the AB-magnitude system (Oke 1974)

$$m_{AB} = -2.5 \log \int f(\nu) e^{-\tau_{eff}} T(\nu) d\nu - 48.6, \qquad (7)$$

where $f(\nu)e^{-\tau_{eff}}$ is the mean incident power measured in ergs cm^{-2} s^{-1} Hz^{-1}, and $T(\nu)$ is the normalized transmittance of the relevant filter. We put our magnitudes directly into the AB system, so that $U_{300} = B_{450} = V_{606} = I_{814}$ corresponds to a spectrum for which $f(\nu)e^{-\tau_{eff}}$ is constant. The observed colors of distant objects are determined by the intrinsic spectral energy distributions (SEDs) of their stellar populations, absorption and scattering of photons in their interstellar media, and stochastic absorption due to intervening H I clouds. Because we do not know when galaxies started forming stars, and over what timescale they formed them, it is impossible to predict their energy distribution in detail. Furthermore, it is not necessarily the case that the faintest galaxies are the most distant. Thus our analysis must not rely on fluxes or apparent magnitudes to give redshift information. It is, however, possible to outline in a general way the range of plausible colors for star-forming galaxies at high redshift, and to identify combinations of age and dust reddening in a stellar population at lower redshift that may conspire to mimic a high-z galaxy.

3.1. The Spectral Energy Distribution of Star-Forming Galaxies

For illustrative purposes, we analyze here two simple examples in detail:

---

[6] Note that ΔU_{300} flattens for $z_{\rm em} \gtrsim 3.6$ because of a significant "red-leak" of the F300W filter above 6700 Å.

(1) We compute the ultraviolet spectrum of a star-forming galaxy using the isochrone synthesis spectral evolutionary code of Bruzual & Charlot (1993). The model has solar metallicity, a constant star formation rate at age 0.3 Gyr, a Salpeter (1955) initial mass function (IMF), $\phi(m) \propto m^{-2.35}$, with lower and upper cutoffs of 0.1 and 125 $M_\odot$, and completely ignores the effects of H I in the local interstellar medium on the transfer of ionizing photons. Two intrinsic discontinuities, about 1.4 mag across the rest-frame Lyman limit and 0.5 mag across the Balmer decrement, are characteristic of the most prominent stars;

(2) We take as fiducial the spectra of the four brightest starburst galaxies observed by the *Hopkins Ultraviolet Telescope* (HUT) on Astro-2: NGC3310, 4214, 5236 and 5253 (Ferguson et al. 1996a). The *HUT* spectra cover the wavelength range $912 < \lambda < 1820$ Å (Kruk et al. 1995). The cutoff at short wavelengths is due to galactic H I . For wavelengths longward of 1820 Å, we have patched on the *IUE* spectra from the Kinney et al. (1993) atlas, renormalized to the *HUT* flux in the range $1350 - 1700$ Å. The renormalization is required because of the different sizes of the *HUT* and *IUE* apertures. Note that the starburst galaxy intrinsic colors are significantly redder than the ones derived from the population synthesis model because of the presence of a large Lyman discontinuity and of dust-reddening. *HUT* spectra of somewhat more distant starbursts galaxies suggest that the intrinsic Lyman break is typically at least a factor of 5 (Leitherer et al. 1995). Analysis of the NGC5236 *HUT* SED suggests that a young ($\sim 5 \times 10^6$ year old) population is responsible for the emission, with an intervening extinction $E(B-V) \approx 0.2$ necessary to fit the detailed SED (Ferguson et al. 1996a). Such a modest extinction appears fairly typical of starburst galaxies (even those of high metallicity). In a comprehensive study of 39 starburst galaxies, Calzetti, Kinney, & Storchi-Bergmann (1994) found values of $E(B-V)$ ranging from 0 to 0.8.

Figure 2a displays the predicted $U_{300} - B_{450}$, $B_{450} - V_{606}$, and $V_{606} - I_{814}$ colors versus emission redshift of our synthetic IGM-attenuated galaxy, together with the unattenuated values. The intrinsic spectral shape has been kept constant with cosmic time. As expected, the observed colors redden quite sharply with redshift due to intergalactic absorption. For example, from $z_{\rm em} = 2.5$ to $z_{\rm em} = 3$, the observed $U_{300} - B_{450}$ color of the Bruzual spectrum increases from 1.8 to 3.6 mag. In the absence of any absorption break, the last value would correspond to a spectral energy distribution $f(\nu) \propto \nu^{-\alpha}$ with $\alpha = 8$.[7] The observed flux decrements between 4500 and 6060 Å and between 6060 and 8140 Å similarly probe the universe at higher and higher redshifts, as $B_{450} - V_{606}$ increases from 0.8 at $z_{\rm em} = 3.5$ to 1.7 mag at $z_{\rm em} = 4$, while $V_{606} - I_{814}$ increases from 1.0 at $z_{\rm em} = 4.5$ to 1.9 mag at $z_{\rm em} = 5$. A similar plot is shown in Figure 2b for the observed *HUT-IUE* starburst galaxy spectra. The main point to note here is how intrinsically blue and red objects follow similar paths in the color-redshift plane, and that, even in the presence of dust-reddening, *the large magnitude jumps between adjacent bandpasses are largely caused by the known sources of intergalactic H I opacity – the Lyα clouds and Lyman-limit systems – rather than by the assumed galaxy SED.*

3.2. Color Selection Criteria

The problem of identifying high redshift galaxies is complicated by the fact that the present-day colors and spectra of galaxies allow for a very wide variety of star-forming histories. This evolution is coupled with chemical evolution of the stars and the ISM and changes in the amount of dust and its distribution relative to the stars. However, galaxy spectra are not entirely arbitrary. Flux is usually a slowly varying function of wavelength, with a few spectral discontinuities (e.g., the 4000 and 912 Å breaks) at specific locations. Thus it should be possible to construct fairly robust selection criteria that will exploit the combined effect of the intrinsic Lyman edge in galaxies and the opacity of intergalactic neutral hydrogen to separate high redshift from low redshift objects.

In this section, we shall define criteria appropriate to the HDF bandpasses. To derive a robust color selection technique, we have computed HDF colors for 1612 synthetic spectra of galaxies, representing

---

[7] Above $z_{\rm em} \approx 3.5$, $U_{300} - B_{450}$ becomes bluer, again an effect of the red-leak of the F300W filter. However, by then, intergalactic attenuation is so strong that high-z galaxies are effectively unobservable in the ultraviolet.

different ages, star formation histories, metallicities, and dust opacities. The stellar-evolutionary input to the models has been described in detail by Babul & Ferguson (1996). Briefly, synthetic spectra are computed using isochrone synthesis from the isochrones of Bertelli et al. (1994), and the model atmospheres of Kurucz (1992) and Clegg & Middlemass (1987). The synthetic spectra agree well with those of Bressan, Chiosi, & Fagotto (1994), which were constructed using the same isochrones, and slightly less well with those of Bruzual & Charlot (1993), primarily due to their use of different isochrones. The uncertainties in population synthesis have been outlined in some detail by Charlot, Worthey, & Bressan (1996). These uncertainties amount to differences in color of several tenths for the same stellar population computed by different codes. While they can cause very large discrepancies in the derived ages, such small variations in color are almost completely negligible for our purposes.

Attenuation by dust has been included using the parametrized extinction laws of Pei (1992) for the Galaxy, the LMC and the SMC. Note that the use of the relatively "gray" extinction curve for starburst galaxies found by Calzetti et al. (1994) would imply a higher UV continuum than predicted on the basis of the optical continuum emission by the application of the standard extinction laws, hence strengthen the efficiency of our selection criteria. We ignore the effects of H I in the local interstellar medium of the galaxies, which will add to the intergalactic attenuation to make high-z objects even redder. There are no emission lines included in the simulations. Given the very wide bandpasses of the HDF filters, we do not expect emission lines to significantly alter galaxy broadband colors.

The colors for the models have been computed at 73 different redshifts spanning the interval $0.001 < z < 7$, taking into account the effect of intergalactic attenuation. In this exercise, galaxies are required to be younger than the age of the universe (for $q_0 = 0.5, H_0 = 50 \, \mathrm{km \, s^{-1} \, Mpc^{-1}}$), but otherwise age has been decoupled from redshift. The model grid is intended to span the range of plausible colors of real galaxies, but not to sample this range in a way that is tied to cosmological models. For example, in the real universe we expect the old, low redshift portion of a color-color diagram to be more densely populated than in our simulations. The adopted grid of ages, star formation timescales, extinctions A_B, and redshifts is summarized in Table 1. It is important to emphasize that our goal is to construct a *robust* set of color selection criteria that are *largely independent* of models of galaxy formation or the assumed values of the cosmological parameters. In this respect our approach is quite distinct from efforts to assign photometric redshifts to each galaxy, as presented by Lanzetta, Yahil, & Fernández-Soto (1996) and Gwyn & Hartwick (1996), for example.

3.2.1. F300W Dropouts

We are now in position to examine the colors of arbitrary galaxies as a function of redshift. Figure 3 shows $U_{300} - B_{450}$ vs. $B_{450} - I_{814}$ for all of the synthetic spectra. The large points show objects with $2 < z < 3.5$. Galaxies in this redshift range predominantly occupy the top left portion of the plot because of the attenuation by the IGM and intrinsic extinction. Galaxies at lower redshift can have similar $U_{300} - B_{450}$ colors, but they are typically either old or dusty, and are therefore red in $B_{450} - I_{814}$ as well. To identify likely star-forming galaxies in our desired redshift range, we require that they have (1) $U_{300} - B_{450} > 1.3$, (2) $U_{300} - B_{450} > B_{450} - I_{814} + 1.2$, and (3) $B_{450} - I_{814} < 1.5$. These criteria isolate objects that have relatively blue colors in the optical, but a sharp drop into the UV.

Figure 4 gives an estimate of the efficiency of this technique. The solid histogram shows the fraction of the total sample of models that meet the selection criteria as a function of redshift. Even with the wide range of parameters in our galaxy models, *no* galaxies with $z < 1.5$ or $z > 4$ are selected. However, many of the galaxies in the redshift range $2 < z < 4$ are missed as well. The galaxies that are missed tend to be redder than the selection line in $B_{450} - I_{814}$, either because they are relatively old, or because they are highly reddened by dust. The dotted histogram in Figure 4 shows the selection efficiency for galaxies with ages restricted to be less than 10^8 yr and extinctions $A_B < 2$. The selection criteria appear to be extremely efficient, recovering roughly 90% of the galaxies in the redshift range $2 < z < 3.5$. Of course the true efficiency depends on how close our models are to real protogalaxies, and on how many old or very dusty

galaxies there are in the real universe in that redshift range.

3.2.2. F450W Dropouts

We can play an identical game with the F450W dropouts. Figure 5 shows the colors of the model galaxies in the $B_{450} - V_{606}$ vs. $V_{606} - I_{814}$ plane, with galaxies in the redshift range $3.5 < z < 4.5$ highlighted, and with our proposed selection criteria drawn. In this case, there are objects outside the redshift range of interest that can have rather blue $V_{606} - I_{814}$ colors and red $B_{450} - V_{606}$ colors, and hence potentially contaminate the sample. These peculiar colors obtain only for those galaxies that lie in the redshift range $2 < z < 3.5$ and have a fair amount of internal extinction. The blue $V_{606} - I_{814}$ color is due to the 2200 Å absorption feature shifting into the F814W bandpass. Our selection criteria are tuned to avoid including many of these galaxies. Specifically, we require our candidates to have (1) $B_{450} - V_{606} > 1.5$, (2) $B_{450} - V_{606} > 1.7(V_{606} - I_{814}) + 0.7$, (3) $B_{450} - V_{606} < 3.5(V_{606} - I_{814}) + 1.5$, and (4) $V_{606} - I_{814} < 1.5$.

Figure 6 shows the fraction of galaxies recovered as a function of redshift for such a selection. Once again, the criteria appear to be very efficient at selecting relatively unreddened star-forming galaxies, this time in the redshift range $3.5 < z < 4.5$. Nevertheless, there is some danger of low redshift contamination for the F450W dropouts. Again, most of the contaminants are either relatively old or reddened galaxies at slightly lower redshift. The dashed histogram in Figure 6 shows the distribution of redshifts for the sample when galaxies are restricted to have either ages greater than 10^9 yr, or $A_B > 2$. Again, the extent of the contamination in the real universe depends on the unknown distribution of dust contents and ages at these redshifts.

4. HIGH REDSHIFT GALAXIES IN THE HUBBLE DEEP FIELD

Using the color selection criteria described above, we shall build in this section a sample of galaxies at high-z selected from the Version 2 catalog of the *Hubble Deep Field*, which is based on the second release of the reduced HDF images. Details of the data reduction, image combination, source detection, and photometry are given by Williams et al. (1996).

Figures $7a$ and $8a$ show color-color plots of the catalog data with our selection region drawn in as dashed lines. The catalog is based on the three WF chips only, and covers an area of 4.65 arcmin². The source detection was carried out on the exposure-weighted sum of the F606W and F814W images, and the threshold was set to 4σ. In all cases, isophotal magnitudes and colors were used for photometry, with identical apertures (defined from a sum of the F606W and F814W images) applied to the images in all bandpasses. It is important to note that the FOCAS isophotal magnitudes are systematic *underestimates* of the true brightness of the galaxies. The magnitude error is difficult to quantify precisely as it depends on the surface brightness profiles of the galaxies in the image. Experiments on simulated data suggest that total magnitudes are typically 0.5 mag brighter than FOCAS isophotal magnitudes (Ferguson et al. 1996b). We have ignored this offset in our analysis, but note that it could increase our inferred luminosity densities and metal production rates by roughly a factor of 1.6. The catalog was truncated at magnitude limits sufficiently bright that Lyman breaks of the expected amplitude could be measured reliably. For the UBI selection, we considered only objects with $B_{450} < 26.79$ and $V_{606} < 28.0$; for the BVI selection, the limiting threshold was set to $V_{606} < 27.67$. Galaxies undetected in F300W (F450W) – as defined by having signal-to-noise ratio < 1 inside the isophotal aperture – were assigned a 1σ lower limit to their $U_{300} - B_{450}$ ($B_{450} - V_{606}$) colors. In the figures, only objects with $I_{814} > 21$ are shown. For the UBI selection of F300W dropout objects, two bright stars (with $I_{814} < 21$) enter into the color selection window. Steidel et al. (1996a) have shown that subdwarf stars may have similar colors to those of $z \sim 3$ galaxies, and indeed Steidel et al. (1996b) confirm that one of the two bright stars in the HDF within this color selection window is indeed a foreground subdwarf star. None of the fainter F300W dropouts appears to be stellar.

The complex, sometimes multi-component morphologies of faint galaxies in deep *HST* images provide a complication for anyone cataloging faint objects in images such as the HDF. Automated object detection routines may break up objects into several components if their light distribution has multiple peaks, and it

is not always clear whether a multi-component object should be considered as a single "parent" entity or split into separate "daughters." We chose to apply our selection criteria to the complete catalog of both parents and daughters, and then inspected all potential high redshift candidates visually. In a few cases, we retained "parents" as single objects (e.g., for the brightest F300W dropout, the elongated object known as C4–06 in the notation of Steidel et al. 1996b), while for others we chose the "daughters" when the parent seemed to comprise distinctly separate objects. Although we shall consider here only the total, summed light from all candidate Lyman break objects, the details of this splitting can be of some importance as the daughters may fall in or out of our sample.

Ultimately, of course, the ability of our color criteria to select largely uncontaminated samples of star-forming galaxies at high-z must be confirmed by deep spectroscopy. In Figures 7b and 8b we plot the location in the color-color diagrams of the more than 60 galaxies in the HDF which have known Keck/LRIS spectroscopic redshifts (Steidel et al. 1996b; Cohen et al. 1996; Moustakas et al. 1996). While none of the low-z objects is found to contaminate our high-z selection regions, our UBI color criteria are able to select 4 of the 5 objects spectroscopically confirmed by Steidel et al. (1996b) to be galaxies in the redshift range $2.591 < z < 3.226$. (Here, photometry from the Version 2 catalogs has been used, whereas Steidel et al. used Version 1 data.) Two out of the six known $z > 2$ objects in the HDF are *not* selected by our criteria. One (a $z = 2.268$ galaxy from the Cohen et al. sample) only just misses being included – its $U - B$ color is slightly bluer than allowed by our color criteria. The second missed source (C4–09 from Steidel et al.) is a more puzzling case – this object is a small diamond-shaped configuration of four distinct sub-components, each of which "disappears" in the F300W bandpass. Steidel et al. considered it as a single object and measured a redshift of 3.23. We fail to identify it as a candidate because it appears as a formal detection (2.7σ) at F300W in the Version 2 catalog, whereas Steidel et al. assigned only an upper limit to its U_{300} flux. This points to some uncertainty in our current understanding of the noise properties of the F300W images, but we do not expect this to significantly impact the results presented here. In the Version 2 catalog, the brightest of the four sub-components of this small "quad" is individually classified as a dropout above our magnitude limit and with the appropriate colors, and is included in the analysis presented here.

4.1. F300W Dropouts: Limits to the Luminosity Density at $2 < z < 3.5$

We have identified 69 F300W dropouts in the HDF images which satisfy the criteria established for star-forming galaxies at $2 < z < 3.5$. Assuming this redshift interval has been uniformly probed, we derive a comoving galaxy number density of $4.2 \times 10^{-3} \, \text{Mpc}^{-3}$ ($0.92 \times 10^{-3} \, \text{Mpc}^{-3}$ for $q_0 = 0.05$) at $\langle z \rangle = 2.75$, about 10 times larger than the comoving space density of bright $L \geq L_*$ present-day galaxies (Loveday et al. 1992). The observed V_{606} magnitudes of our sample yield a specific (comoving) emissivity at 1620 Å equal to

$$\rho_{1620} \approx 1.6 \times 10^{26} \, \text{ergs} \, \text{s}^{-1} \, \text{Hz}^{-1} \, \text{Mpc}^{-3} \tag{8}$$

($9.0 \times 10^{25} \, \text{ergs} \, \text{s}^{-1} \, \text{Hz}^{-1} \, \text{Mpc}^{-3}$ for $q_0 = 0.05$). The faintest F300W dropout has a magnitude of $V_{606} = 26.7$, corresponding, in the case of a flat-spectrum source at $\langle z \rangle = 2.75$, to a B-band luminosity of about $0.1L_*$, or a total star formation rate (Salpeter IMF) of $\sim 1 \, \text{M}_\odot \, \text{yr}^{-1}$. The brightest has $V_{606} = 23.6$, and is forming stars at a rate of $\sim 20 \, \text{M}_\odot \, \text{yr}^{-1}$.

It is interesting to compare the comoving space density of the HDF F300W dropouts brighter than $V_{606} = 25$, $7.3 \times 10^{-4} \, \text{Mpc}^{-3}$ at $\langle z \rangle = 2.75$, with that derived from Steidel et al. (1996a) ground-based statistic, $3.6 \times 10^{-4} \, \text{Mpc}^{-3}$ to $\mathcal{R} < 25$ at redshift $\langle z \rangle = 3.25$. Within the errors, the two estimates appear in good agreement with one another, especially after accounting for the fact that one probes ~ 0.3 mag fainter in the galaxy luminosity function at the HDF average redshift.

4.2. F450W Dropouts: Limits to the Luminosity Density at $3.5 < z < 4.5$

In a similar manner, we have identified 14 F450W dropouts which satisfy the criteria established for star-forming galaxies at $3.5 < z < 4.5$. Their comoving number density at $\langle z \rangle = 4.0$ is $1.5 \times 10^{-3} \, \text{Mpc}^{-3}$ ($2.4 \times 10^{-4} \, \text{Mpc}^{-3}$ for $q_0 = 0.05$). From the observed I_{814} magnitudes, we derive a specific (comoving)

emissivity at 1630 Å of

$$\rho_{1630} \approx 5.0 \times 10^{25} \, \mathrm{ergs \, s^{-1} \, Hz^{-1} \, Mpc^{-3}} \tag{9}$$

$(2.8 \times 10^{25} \, \mathrm{ergs \, s^{-1} \, Hz^{-1} \, Mpc^{-3}}$ for $q_0 = 0.05$). The faintest F450W dropout has a magnitude of $I_{814} = 27.5$, corresponding, in the case of a flat-spectrum source at $\langle z \rangle = 4$, again to a B-band luminosity of about $0.1 L_*$, while the brightest has $I_{814} = 25$. Our samples of U_{300} and B_{450} dropouts therefore reach comparable depths. *We stress that, contrary to the case at $2 < z < 3.5$, we have yet no spectroscopic confirmation of the efficiency of our color-selection criteria at $3.5 < z < 4.5$.*

The source catalogs of the U_{300} and B_{450} dropouts are presented in Tables 2 and 3. For each galaxy we report the FOCAS catalog entry number from Williams et al. (1996) (ID), the right ascension and declination (α, δ), and the AB isophotal magnitudes in the four HDF passbands.[8] The UV dropouts 2-449.0, 3-550.0, 4-555.1, and 4-676.0 have been spectroscopically identified by Steidel et al. (1996b) as galaxies at $z = 2.845$, 2.775, 2.803, and 2.591, respectively.

5. COSMIC STAR FORMATION HISTORY

The results of the Canada-France Redshift Survey (CFRS, Lilly et al. 1995) over the redshift range $0 < z < 1$, the spectroscopic confirmation by Steidel et al. (1996a,b) of the existence of a substantial population of luminous, star-forming galaxies at $2.5 < z < 3.5$, together with our statistical constraints on the redshift distribution of faint galaxies in the *Hubble Deep Field*, as derived above for $2 < z < 4.5$, have considerable implications for our understanding of the global history of star and structure formation in the universe. Here, we review some of the consequences of these observations, focusing on what can be learned about galaxy evolution at early (and late) epochs from integrated quantities over the entire population, rather than from a detailed study of individual objects.

5.1. The Metal Production Density of the Universe

The UV continuum emission from a galaxy with significant ongoing star formation is totally dominated by short-lived massive stars, and is therefore nearly independent of the galaxy history. Moreover, the (rest-frame) radiation flux below 3000 Å is a very good measurement of the instantaneous ejection rate of heavy elements ($Z \geq 6$), since both are directly related to the number of massive stars (Cowie 1988; Songaila, Cowie, & Lilly 1990; Madau & Shull 1996): the same stars with $m > 10 \, \mathrm{M_\odot}$ that manufacture and return most of the metals to the ISM also dominate the UV light. The supernova event from a star of $25 \, \mathrm{M_\odot}$ injects about $4.5 \, \mathrm{M_\odot}$ of metals (Woosley & Weaver 1995). At the end of the C-burning phase $\sim 17 \, \mathrm{M_\odot}$ have been converted into helium and carbon (Maeder 1992), with a mass fraction released as radiation of 0.007. For each $1 \, \mathrm{M_\odot}$ of metals ejected, to first approximation we then expect $(17 \times 0.007/4.5) = 0.025 \, \mathrm{M_\odot} \, c^2$ of energy to be radiated away.

What we are interested in here is the universal rate of ejection of newly synthesized material per unit comoving volume. In the approximation of instantaneous recycling, the metal ejection rate (MER) per unit volume can be written as (cf Tinsley 1980)

$$\dot{\rho}_Z = \psi \int m p_{\mathrm{zm}} \phi(m) dm, \tag{10}$$

where ψ is the star formation rate (SFR) density, $\phi(m)$ is the IMF (normalized through the relation $\int m \phi(m) dm = 1$), and p_{zm} is the stellar yield, i.e., the mass fraction of a star of mass m that is converted

---

[8] The use of a more conservative criterion which assigns a 2σ lower limit to the $U_{300} - B_{450}$ colors of galaxies undetected in the F300W bandpass would decrease the number of ultraviolet dropouts to 47, thereby decreasing the integrated emissivity given in eq. (8) by a factor of 1.3. The same 2σ color criterion applied to galaxies undetected in F450W decreases to only 9 the number of blue dropouts, resulting in an emissivity which is a factor 1.4 lower than that given in eq. (9).

to metals and ejected. The dot denotes differentiation with respect to cosmic time. At short wavelengths, the luminosity density radiated per unit frequency during the main sequence phase is related to ψ by

$$\rho_\nu = 0.007c^2\psi \int m f_{\mathrm{He}}(m) f_\nu(m) \phi(m) dm, \tag{11}$$

where $f_{\mathrm{He}}(m)$ is the mass fraction of hydrogen burned into helium, and $f_\nu(m)$ is the normalized spectrum of stars of mass m on the main sequence. The detailed conversion from UV luminosity to MER, including all evolutionary stages, can be obtained from spectral synthesis and metal-yield calculations. For simplicity, we shall ignore here the contributions of planetary nebulae (Renzini & Voli 1981), Type Ia supernovae (Thielemann, Nomoto, & Yokoi 1986), and stellar winds (Maeder 1992) to the chemical yields, and focus on the nucleosynthetic enrichment by supernova explosions from massive stars. We use the evolutionary models of Bruzual & Charlot (1993) and the Type II stellar yields tabulated by Woosley & Weaver (1995) (see also Sutherland & Shull 1996). For a Salpeter IMF including stars in the $0.1 < M < 125\,\mathrm{M_\odot}$ mass range, a constant SFR, a galaxy age in the interval 0.1–1 Gyr, and solar metallicity, we derive

$$\rho_{1500} = 4.4 \pm 0.2 \times 10^{29}\dot{\rho}_Z \ \ \mathrm{ergs\,s^{-1}\,Hz^{-1}\,Mpc^{-3}} \tag{12}$$

at $1500\,\text{Å}$, and

$$\rho_{2800} = 2.8 \pm 0.3 \times 10^{29}\dot{\rho}_Z \ \ \mathrm{ergs\,s^{-1}\,Hz^{-1}\,Mpc^{-3}} \tag{13}$$

at $2800\,\text{Å}$, where $\dot{\rho}_Z$ is the MER in $\mathrm{M_\odot\,yr^{-1}\,Mpc^{-3}}$. The continuum spectrum is fairly flat and is dominated by early-type stars. We shall use the relations given above in the subsequent discussion, while noting that the conversion efficiency is fairly insensitive to the assumed IMF (as long as the stellar population extends as a power-law to massive stars, 50–100 $M_\odot$), since the increased metal yield from high mass stars is compensated for by a similar increase in the production of UV photons. The advantage then of deriving from the observed UV luminosity density a rate of metal ejection, rather than a SFR, is that the latter is instead a sensitive function of the IMF slope. To be quantitative, while for a Salpeter IMF the mean yield of returned metals is

$$\int m p_{\mathrm{zm}}\phi(m)dm = 2.4\%, \tag{14}$$

for a Scalo (1986) IMF – less rich in massive stars – in the same mass range this factor is about 3.3 times lower. Hence large errors in the relative rates of star formation at different epochs may occur if the IMF varies with cosmic time. Because of these considerations, unless otherwise stated we shall only quote metal ejection rates in the following. Note, however, that the real uncertainties in the UV-to-metal conversion factors due to age, IMF, metallicity, and population synthesis model well exceed the errors quoted above.

To relate the amount of heavy elements observed today in various stellar populations and in the gas phase to the UV luminosity of distant, star-forming galaxies, we may use the conservation of metals, which implies that the sum of the heavy elements stored in stars, $Z_*\rho_*$, and in the gas, $Z_g\rho_g$, is equal to the mass of metals ever ejected, i.e., to the integral of equation (10) over cosmic time. An estimate of the baryonic mass in galaxies can be obtained by multiplying the observed luminosity density of the local universe by a mass-to-light ratio. Since the gaseous content of nearby galaxies is observed to be negligible compared with the stellar content (e.g., Rao & Briggs 1993), the cosmological mass density of heavy elements at the present epoch is given by

$$\rho_Z(0) \approx Z_*\rho_*(0) = Z_*\rho_B(0)(\frac{M}{L_B}), \tag{15}$$

where $\rho_B(0)$ is the local blue light density of field galaxies, and M/L_B is the mass-to-blue light ratio of visible matter. There are several recent determinations of the B-band luminosity density from large redshift surveys. The values obtained for $\log \rho_B(0)$ in units of $\mathrm{L_\odot\,Mpc^{-3}}$ are 7.98 (Efstathiou, Ellis, & Peterson

1988), 7.83 (Loveday et al. 1992), 8.0 (Marzke, Huchra, & Geller 1994), 7.93 (da Costa et al. 1994), and 8.0 (Ellis et al. 1996). A simple average of all these determinations gives the adopted value:

$$\rho_B(0) = 9.0 \pm 1.4 \times 10^7 \, \mathrm{L_\odot \, Mpc^{-3}}. \tag{16}$$

The mass-to-light ratios for the visible parts of galaxies can be estimated from stellar population modeling. The results (in solar units) are in the range $2 < M/L_B < 6$, the smaller value referring to a typical Population I system like the solar neighborhood (e.g., Kuijken & Gilmore 1989), the larger value to the old stellar populations of elliptical galaxies (e.g., van der Marel 1991). Since about 30% of the total blue luminosity density is in ellipticals (Efstathiou et al. 1988), we may adopt the luminosity-weighted mean value of $\langle M/L_B \rangle = 3$ to derive

$$\rho_Z(0) \approx 5.4 \pm 0.8 \times 10^6 (\frac{Z_*}{Z_\odot}) \, \mathrm{M_\odot \, Mpc^{-3}} \tag{17}$$

(cf Cowie 1988). While representative stellar metallicities in nearby luminous spirals and ellipticals are approximately solar, $Z_* \sim Z_\odot = 0.02$, irregular, blue compact, and dwarf spheroidal galaxies are known to be metal poor, $Z_* \gtrsim 0.1 Z_\odot$ (e.g., Pagel & Edmunds 1981).

The real uncertainty on the metal mass density is difficult to estimate, but is unlikely to exceed a factor of 1.5. Although a baryonic mass several times larger than the luminous mass may be present in the Galactic halo, metal-rich halo material would be mixed into and over-enrich the disk. Hence, if a substantial amount of metals are missing from our census, they are most likely hidden in low-surface brightness galaxies (Ferguson & McGaugh 1995), or intergalactic and intracluster gas.

It is useful at this stage to define a fiducial metal ejection density,

$$\dot{\Sigma}_Z = \rho_Z(0) t_H(0)^{-1} \approx 4.2 \times 10^{-4} \, \mathrm{M_\odot \, yr^{-1} \, Mpc^{-3}}, \tag{18}$$

given by the present-day mass density in heavy elements divided by the current age of the universe. If $\dot{\rho}_Z$ observed at a given redshift z is much less than $\dot{\Sigma}_Z$, and a large fraction of the luminous baryons observed today were already locked into galaxies at this epoch, then either galaxies have already exhausted their reservoirs of cold gas or there must be a mechanism which prevent the gas within virialized dark matter halos to radiatively cool and turn into stars. By contrast, a metal ejection rate much greater than the fiducial value implies that the conversion of gas into stars can be extremely efficient at times. From a comparison between the observed $\dot{\rho}_Z$ and $\dot{\Sigma}_Z$ we may then be able to distinguish between a more or less uniform (with cosmic time) SFR and a discontinuos one, consisting of a series of bursts of suitable duty cycle.

According to Gallego et al. (1995), the Hα luminosity density of the local universe is $\rho_{\mathrm{H}\alpha}(0) = 1.3 \pm 0.6 \times 10^{39} \, \mathrm{ergs \, s^{-1} \, Mpc^{-3}}$. This value implies[9] a MER at the present epoch of

$$\dot{\rho}_Z(0) \approx 1.1 \pm 0.5 \times 10^{-4} \, \mathrm{M_\odot \, yr^{-1} \, Mpc^{-3}}. \tag{19}$$

Equations (18) and (19) suggest that the present rate of production of heavy elements is too low to yield the observed element abundances in the Hubble time, and that either star-forming galaxies were much more numerous in the past, or individual galaxies must, on average, have passed through a significantly brighter phase.

---

[9] In case-B recombination theory, the Hα luminosity density can be related to the emission rate of ionizing photons per unit cosmic volume, $\dot{n}_{\mathrm{ion}}$, according to $\rho_{\mathrm{H}\alpha} \approx 0.45 h \nu_{\mathrm{H}\alpha} \dot{n}_{\mathrm{ion}}$ (Osterbrock 1989). Population synthesis galaxy spectra (Bruzual & Charlot 1993) with constant SFR yield the following approximate relation between ρ_{1500} and $\dot{n}_{\mathrm{ion}}$: $\dot{n}_{\mathrm{ion}} \approx 0.14 \rho_{1500}/h$, nearly independent of age in the interval 0.1–1 Gyr.

From the CFRS faint galaxy survey (Lilly et al. 1995), we now know that the MER per unit mass was in fact considerably larger in the past. The comoving metal ejection density at $0 < z < 1$ corresponding to the observed specific luminosity density at $2800\,\text{Å}$ (the "LF-estimated" value of Lilly et al. 1996) is

$$\dot{\rho}_Z(z) \approx 1.5 \pm 0.6 \times 10^{-3} \left(\frac{1+z}{2}\right)^{3.9} \text{M}_\odot \, \text{yr}^{-1} \, \text{Mpc}^{-3}, \tag{20}$$

about 15 times higher at $z \sim 1$ than the current value. This strong evolution is associated with galaxies bluer than typical Sbc's. The luminosity function of redder galaxies shows little change back to $z \sim 1$.

The sample of Lyman-break star-forming galaxies identified by Steidel et al. (1996a) has a comoving density of $\approx 3.6 \times 10^{-4}\,\text{Mpc}^{-3}$ at $\langle z \rangle = 3.25$, and an average continuum specific luminosity at $1500\,\text{Å}$ of $10^{41}\,\text{ergs s}^{-1}\,\text{Å}^{-1}$. This gives a comoving volume emissivity of $2.7 \times 10^{25}\,\text{ergs s}^{-1}\,\text{Hz}^{-1}\,\text{Mpc}^{-3}$, hence a MER density

$$\dot{\rho}_Z(3.25) \approx 6.2 \times 10^{-5} \, \text{M}_\odot \, \text{yr}^{-1} \, \text{Mpc}^{-3}, \tag{21}$$

comparable with the local value but more than 20 times lower than the $z = 1$ one. [10]

Finally, our analysis of the HDF images yields, from equations (8) and (9):

$$\dot{\rho}_Z(2.75) \approx 3.6 \times 10^{-4} \, \text{M}_\odot \, \text{yr}^{-1} \, \text{Mpc}^{-3}, \tag{22}$$

and

$$\dot{\rho}_Z(4) \approx 1.1 \times 10^{-4} \, \text{M}_\odot \, \text{yr}^{-1} \, \text{Mpc}^{-3}. \tag{23}$$

Note that the MER density at $\langle z \rangle = 2.75$ is more than a factor of 5 larger than the Steidel et al. (1996a) ground-based value at $\langle z \rangle = 3.25$, largely because the HDF deep images probe about 1.7 mag fainter into the rest-frame luminosity function at these redshifts. Still, the derived luminosity density is significantly smaller than the rate at $z \approx 1$. It is conceivable that our list of candidates in the HDF may be sampling a significant fraction of the galaxy luminosity function at these redshifts, and that the contribution to the luminosity density from galaxies below our magnitude threshold is small. Strictly speaking, however, the metal ejection rates derived above from the HDF data (and the emissivities given in eqs. [8] and [9]) should be interpreted as lower limits to the real values, as they only include the fraction arising in the most actively star-forming, young and nearly dust-free objects. The same considerations also apply to the sample identified by Steidel et al. (1996a). We point out that large numbers of faint galaxies at high redshifts are quite plausible in cold dark matter-like cosmologies, because of the high space density of low mass dark matter halos predicted in any hierarchical theory of galaxy formation (e.g., White & Frenk 1991).

The derived star and element formation history of the universe is depicted in Figure 9. Although the star formation densities beyond $z = 2$ are only lower limits, together with the Gallego et al. and Lilly et al. values they seem consistent with the existence of a peak in the cosmic metal production rate in the redshift range $1 \lesssim z \lesssim 2$, as predicted by models of the chemical evolution of the damped Lyα absorption systems (Pei & Fall 1995).

5.2. Clues to Galaxy Formation and Evolution

We may at this stage try to establish a cosmic timetable for the production of heavy elements in relatively bright galaxies, keeping in mind the inherent uncertainties associated with the estimates given above. In an Einstein-de Sitter universe, the total mass density processed into metals over the redshift range $0 < z < z_c \approx 1$, is, integrating equation (20) over cosmic time,

$$\Delta\rho_Z(0) = (8.2 \pm 2.6 \times 10^5 \, \text{M}_\odot \, \text{Mpc}^{-3})[(1 + z_c)^{2.4} - 1] = 3.5 \pm 1.1 \times 10^6 \, \text{M}_\odot \, \text{Mpc}^{-3}. \tag{24}$$

---

[10] Note that the star formation density at $z = 0$ quoted by Gallego et al. (1995) is derived assuming a Scalo IMF, while Steidel et al. (1996a) adopt a Salpeter IMF in their paper.

(Contrary to the measured number densities of objects and rates of star formation, the metal mass density does not depend on the assumed cosmological model.) If we define two characteristic epochs of star and element formation in galaxies, z_* and z_Z, as the redshifts by which half of the current stellar and metal content of galaxies was formed, then a straightforward comparison between equations (17) and (24), together with the fact that most of the stars in the inner luminous parts of galaxies are metal rich, imply $z_* \lesssim z_Z \approx 1$, or in other words that a significant fraction of the current metal content of galaxies was formed relatively late, on a timescale of about 8 Gyr. This is comparable with the decay time of star formation, from 5 to 9 Gyr, required to reproduce the present-day colors of late-type spirals (e.g., Bruzual & Charlot 1993), and suggests the possibility that we may be observing in the redshift range $z = 0 - 1$ the conversion into stars of gaseous galactic disks. Pure H I disks may be assembled at some higher redshift, and disk gas continuosly replenished as a result of ongoing infall from the surrounding hot halo. The case for a "disk epoch" at $z \sim 1$ is strengthened by the observations that galaxies of different luminosities and morphological type evolve very differently. A common conclusion of several recent deep redshift surveys (e.g., Glazebrook et al. 1995; Lilly et al. 1995; Ellis et al. 1996) is that late-type, gas-rich systems show substantial evolution in number and/or luminosity from the present to $z \sim 1$, and that a large fraction of the observed evolution is associated with an increase in the mean surface brightness of luminous disks (Schade et al. 1995). By contrast, the ellipticals and early-type spirals have been remarkably quiescent over the same redshift interval.

From stellar population studies we also know that about half of the present-day stars – hence metals – are contained into spheroidal systems, i.e., elliptical galaxies and spiral galaxy bulges, and that these formed early and rapidly. The major arguments come from studies of Galactic bulge color-magnitude diagrams (Ortolani et al. 1995) which indicate ages as old as globular clusters, and from studies of the chemical abundances in cluster ellipticals and cluster X-ray gas, whose high α-element ratios suggest that both the stars and the intracluster gas must have been enriched on timescales of order 1 Gyr or less (Renzini et al. 1993). If these arguments are correct (and they are by no means undisputed), then bulges and ellipticals must have experienced a bright starburst phase at high z. Where are these protospheroids?

There are a few circumstantial pieces of evidence supporting the interpretation that the Lyman-break galaxies identified at $z > 2.5$ from ground-based images may represent the progenitors of present-day luminous galaxies while forming their spheroidal stellar component. From the strength of their interstellar UV absorption lines, and within the assumption that their velocity field is dominated by gravity, Steidel et al. (1996a) have shown that galaxies at $z \sim 3$ have masses comparable to that of present-day L_* galaxies. Smaller masses would result if interstellar shocks, local to the star-forming regions, contribute significantly to the velocity field. While the *HST* images of these galaxies show the presence of compact (half-light radii of 0.2–0.3 arcsec) cores (Giavalisco et al. 1996), from the deeper HDF data is seems that the F300W dropouts may be better described as asymmetric or irregular objects (Abraham et al. 1996; van den Bergh et al. 1996).

The observations described above may confirm the rationale that galaxies form stars from the inside out, i.e., that spheroidal systems have assembled rather early, far beyond the disk epoch at $z \sim 1$. At the star formation density levels inferred from the HDF images at $\langle z \rangle = 2.75$ (see eq. [22]) about 15% of the observed mass density of metals at $z = 0$ would have been formed during the "spheroid epoch" at $z \gtrsim 2$. This fraction could increase if the star formation is shrouded in dust or takes place in galaxies small enough individually to fall below the HDF source detection limit. On the other hand, since the metals we observe being formed are a substantial fraction of the entire metal content of galaxies, *it appears that star formation regions remain largely unobscured by dust throughout much of galaxy formation.*

With the data presented here, two arguments which have implications for models of galaxy formation can be made more quantitative.

• From Efstathiou et al. (1988), the space density of bright ellipticals today is $n(> L_*) = 2.4 \times 10^{-4} \, \mathrm{Mpc}^{-3}$. If a significant fraction of their stellar population formed in a single burst of duration 1 Gyr early in the history of the universe, a comparable number density of objects should be observed at high-z

while forming stars at rates in excess of $50 - 100\,\mathrm{M_\odot\,yr^{-1}}$. We find that none of the HDF F300W dropouts spectroscopically confirmed by Steidel et al. (1996b) has a SFR in excess of $20\,\mathrm{M_\odot\,yr^{-1}}$ (Salpeter IMF). Assuming a probed redshift interval between 2 and 3.5, we can set an upper limit to the comoving density of very high star-forming galaxies at $\langle z \rangle = 2.75$, $n(> 20\,\mathrm{M_\odot yr^{-1}}) < 6 \times 10^{-5}\,\mathrm{Mpc^{-3}}$. Hence there appears to be a deficit of very bright objects relative to the expectations of the standard early-and-rapidly-forming picture for spheroidal systems.

• In hierarchical models of galaxy formation, small objects form first and merge together to make larger ones. While much of the activity associated with star formation and galaxy merging occurs at relatively low redshifts (White & Frenk 1991), there is no period when bulges and ellipticals form rapidly as single units and are very bright: rather, galaxies become progressively less luminous, more numerous, and more compact at earlier epochs. A common prediction of hierarchical models appears to be the steepening with lookback time of the luminosity function due to the large increase of the abundance of objects forming stars at modest rates (e.g, Cole et al. 1994). It is then interesting to compare, as a function of redshift, the ratio of the space densities of galaxies forming stars at rates in excess of, say, 1 and 10 $\mathrm{M_\odot\,yr^{-1}}$. From the Gallego et al. (1995) Hα survey, we estimate $n(> 1\,\mathrm{M_\odot yr^{-1}})/n(> 10\,\mathrm{M_\odot yr^{-1}}) \approx 50$ at the present epoch. A similar value is found to characterize, at $\langle z \rangle = 2.75$, the distribution of SFRs of the F300W dropouts in the HDF. Thus, unless a substantial fraction of the modest star-forming galaxies at these early times are red either because are relatively old or because are reddened by dust, there seems to be little evidence in our sample for a large enhancement of their space density relative to the abundance of high star-forming objects.

5.3. Chemical Enrichment of the Intergalactic Medium

There is one piece of evidence pointing towards a metal ejection density at $z \gtrsim 3$ which is at least as large as derived in equation (22), namely the observations of a significant cosmological mass density of metals associated with QSO absorption systems at high-z. We shall focus here on the numerous Lyα forest clouds. Recent spectra at high S/N and resolution obtained with the Keck telescope (Tytler et al. 1995; Cowie et al. 1995) have shown that 50%–60% of the Lyα clouds with $\log N_{\mathrm{HI}} > 14.5$ have undergone some chemical enrichment, as evidenced by weak, but measurable C IV absorption lines. The typical inferred metallicities, Z_{IGM}, range from 0.003 to 0.01 of solar values, subject to uncertainties of photoionization models. Because the Lyα clouds have large filling factors and contain a significant fraction of the baryons in the universe, the new data are strong evidence for a widespread distribution of metals in the IGM. These metals may have been produced in situ or in dense gaseous regions of galaxies; the metal-enriched gas was then expelled from the regions of star formation to large distances consistent with the sizes of the Lyα clouds.

Associated with the latter type of enrichment a characteristic MER density can be estimated as

$$\dot\rho_{Z,\mathrm{IGM}}(3) \approx (4 \times 10^{-4}\,\mathrm{M_\odot\,yr^{-1}\,Mpc^{-3}}) \left(\frac{\Omega_{\mathrm{IGM}}}{0.05}\right)\left(\frac{Z_{\mathrm{IGM}}}{0.005 Z_\odot}\right)\left(\frac{f_{\mathrm{inj}}}{0.5}\right)^{-1}\left(\frac{\Delta t}{t_H}\right)^{-1}, \tag{25}$$

where Ω_{IGM} is the baryonic density parameter of the Lyα cloud phase, f_{inj} is the fraction of heavy elements injected into the IGM during a timescale Δt, and t_H is the Hubble time at $z = 3$. If QSO absorption systems trace the bulk of star formation occurring in galaxies at high redshifts (Lanzetta, Wolfe, & Turnshek 1995; Pei & Fall 1995; Madau & Shull 1996), it is therefore plausible that a population of dwarf galaxies, actively forming stars at $z \gtrsim 3$ at a rate comparable to the limit inferred from the HDF data, may be responsible for the contamination of the IGM at high redshifts. Such galaxies have shallow gravitational potential wells, thus allowing easy ejection of the heavy elements produced during their active star-forming phase.

5.4. The Ionizing Background at $z \gtrsim 4$

In the last few years growing evidence has accumulated on the existence of a significant decline in the space density of bright QSOs beyond $z \sim 3$ (Schneider, Schmidt, & Gunn 1994; Warren, Hewett, & Osmer 1994; Kennefick, Djorgovski, & de Carvalho 1995). This shortfall, estimated to be about a factor of 5, poses serious problems to the idea that a quasar-dominated UV background is responsible for maintaining

the intergalactic gas in a highly ionized state above $z \sim 4$ (e.g., Haardt & Madau 1996). It may be of some interest, in this context, to speculate on the possible contribution of our population of star-forming "spheroids" to the metagalactic flux at early epochs (see also Songaila et al. 1990). A minimum value for the intensity of the ionizing background at $z = 4$ is given by

$$J_L(4) = \frac{hc}{4\pi} n_{\mathrm{H,crit}}(4)\Omega_{\mathrm{IGM}} \approx 2.4 \times 10^{-22} \left(\frac{\Omega_{\mathrm{IGM}}}{0.05} \right) \mathrm{ergs\, cm^{-2}\, s^{-1}\, Hz^{-1}\, sr^{-1}}, \qquad (26)$$

where $n_{\mathrm{H,crit}}$ is the closure hydrogen density. This equation reflects the underlying physics of the ionization process: ignoring recombinations, at least one UV photon is required per hydrogen atom to photoionize the IGM. The ionizing radiation flux is largely local, as sources at higher redshifts are severely absorbed by intervening clouds. At $z = 4$, the attenuation length is only $\Delta l \approx 13\,\mathrm{Mpc}$ (Madau 1992). The required (proper) volume emissivity at 1 ryd is then $4\pi J_L/\Delta l$. Collecting, and converting as usual an ionizing luminosity density into a MER per unit comoving volume, we obtain

$$\dot{\rho}_{Z,\mathrm{ion}}(4) \approx (2 \times 10^{-4}\,\mathrm{M_\odot\, yr^{-1}\, Mpc^{-3}}) \left(\frac{\Omega_{\mathrm{IGM}}}{0.05} \right) \left(\frac{f_{\mathrm{esc}}}{0.5} \right)^{-1}, \qquad (27)$$

where now f_{esc} is the escape fraction into the IGM of Lyman-continuum photons. A comparison between equations (23) and (27) provides some rationale for the hypothesis that a population of galaxies at $z \sim 4$, producing metals at a rate which is a few times higher than the lower limit derived from the HDF data, might rival quasars as a source of photoionization of the IGM. Larger star formation rates would be required if a significant fraction of the UV radiation emitted from stars cannot escape into the intergalactic space, $f_{\mathrm{esc}} \ll 1$.

REFERENCES

Abraham, R. G., Tanvir, N. R., Santiago, B. X., Ellis, R. S., Glazebrook, K., & van den Bergh, S. 1996, MNRAS, in press

Babul, A., & Ferguson, H. C. 1996, ApJ, 458, 100

Bertelli, G., Bressan, A., Chiosi, C., Fagotto, F., & Nasi, E. 1994, A&AS, 106, 275

Bressan, A., Chiosi, C., & Fagotto, F. 1994, ApJS, 94, 63

Bruzual, A. G., & Charlot, S. 1993, ApJ, 405, 538

Calzetti, D., Kinney, A. L., & Storchi-Bergmann, T. 1994, ApJ, 429, 582

Charlot, S., Worthey, G., & Bressan, A. 1996, ApJ, 457, 625

Clegg, R. E. S., & Middlemass, D. 1987, MNRAS, 228, 759

Cohen, J. G., Cowie, L. L., Hogg, D. W., Songaila, A., Blandford, R., Hu, E. M., & Snopbell, P. 1996, submitted to ApJ

Cole, S., Aragón-Salamanca, A., Frenk, C. S., Navarro, J. F., & Zepf, S. E. 1994, MNRAS, 271, 781

Cowie, L. L. 1988, in The Post-Recombination Universe, ed. N. Kaiser and A. Lasenby (NATO Advanced Science Institute Series), p. 1

Cowie, L. L., Songaila, A., Kim, T.-S., & Hu, E. M. 1995, AJ, 109, 1522

da Costa, L. N., et al. 1994, ApJ, 424, L1

Djorgovski, S., & Thompson, D. 1993, in IAU Symp. 149, The Stellar Populations in Galaxies, eds. A. Renzini & B. Barbuy (Dordrecht: Kluwer), 337

Efstathiou, G., Ellis, R. S., & Peterson, B. A. 1988, MNRAS, 232, 431

Ellis, R. S., Colless, M., Broadhurst, T., Heyl, J., & Glazebrook, K. 1996, MNRAS, 280, 235

Ferguson, H. C., et al. 1996a, in preparation

———— . 1996b, in preparation

Ferguson, H. C., & McGaugh, S. S 1995, ApJ, 440, 470

Gallagher, J. S., Bushouse, H., & Hunter, D. A. 1989, AJ, 97, 700

Gallego, J., Zamorano, J., Aragón-Salamanca, A., & Rego, M. 1995, ApJ, 455, L1

Giavalisco, M., Steidel, C. C., & Macchetto, F. D 1996, ApJ, in press

Glazebrook, K., Ellis, R. S., Santiago, B. X., & Griffith, R. 1995, MNRAS, 275, L19

Guhathakurta, P., Tyson, J. A., & Majewski, S. R. 1990, ApJ, 357, L9

Gwyn, S. D. J., & Hartwick, F. D. A. 1996, ApJ, in press

Haardt, F., & Madau, P. 1996, ApJ, 461, 20

Kennefick, J. D., Djorgovski, S. G., & de Carvalho, R. R. 1995, AJ, 110, 6

Kennicutt, R. C. 1992, ApJ, 388, 310

Kinney, A. L., Bohlin, R. C., Calzetti, D., Panagia, N., & Wyse, R. F. G. 1993, ApJS, 86, 5

Kruk, J. W., et al. 1995, ApJ, 454, L1

Kuijken, K., & Gilmore, G. 1989, MNRAS, 239, 605

Kurucz, R. L. 1992, private communication

Lanzetta, K. M., Yahil, A., & Fernández-Soto, A. 1996, Nature, 381, 759

Lanzetta, K. M., Wolfe, A. M., & Turnshek, D. A. 1995, ApJ, 440, 435

Leitherer, C., Ferguson, H. C., Heckman, T. M., & Lowenthal, J. D. 1995, ApJ, 454, L19

Lilly, S. J., Tresse, L., Hammer, F., Crampton, D., & Le Févre, O. 1995, ApJ, 455, 108

Lilly, S. J., Le Févre, O., Hammer, F., & Crampton, D., 1996, ApJ, 460, L1

Loveday, J., Peterson, B. A., Efstathiou, G., Maddox, S. J. 1992, ApJ, 390, 338

Madau, P. 1992, ApJ, 389, L1

——— . 1995, ApJ, 441, 18

Madau, P., & Shull, J. M. 1996, ApJ, 457, 551

Maeder, A. 1992, A&A, 264, 105

Marzke, R. O., Huchra, J. P., & Geller, M. J. 1994, ApJ, 428, 43

Møller, P., & Jakobsen, P. 1990, A&A, 228, 299

Moustakas, L., Zepf, S., & Davis, M. 1996, http://astro.berkeley.edu/davisgrp/HDF

Oke, J. B. 1974, ApJS, 27, 21

Ortolani, S., Renzini, A., Gilmozzi, R., Marconi, G., Barbuy, B., Bica, E., & Rich, M. R. 1995, Nature, 377, 701

Osterbrock, D. E. 1989, Astrophysics of Gaseous Nebulae and Active Galactic Nuclei (Mill Valley: University Science Books)

Pagel, B. E. J., & Edmunds, M. G. 1981, ARA&A, 19, 77

Pei, Y. C. 1992, ApJ, 395, 130

Pei, Y. C., & Fall, S. M. 1995, ApJ, 454, 69

Press, W. H., Rybicki, G. B., & Schneider, D. P. 1993, ApJ, 414, 64

Pritchet, C. J., & Hartwick, F. D. A. 1990, ApJ, 355, L11

Rao, S. & Briggs, F. 1993, ApJ, 419, 515

Renzini, A., Ciotti, L., D' Ercole, A., & Pellegrini, S. 1993, ApJ, 419, 52

Renzini, A., & Voli, M. 1981, A&A, 94, 175

Salpeter, E. E. 1955, ApJ, 121, 161

Schade, D., Lilly, S. J., Crampton, D., Le Févre, O., Hammer, F., & Tresse, L. 1995, ApJ, 451, L1

Schneider, D. P., Schmidt, M., & Gunn, J. E. 1991, AJ, 101, 2004

——— . 1994, AJ, 107, 1245

Songaila, A., Cowie, L. L., & Lilly, S. J. 1990, ApJ, 348, 371

Steidel, C. C., Giavalisco, M., Pettini, M., Dickinson, M., & Adelberger, K. L. 1996a, ApJ, 462, L17

Steidel, C. C., Giavalisco, M., Dickinson, M., & Adelberger, K. L. 1996b, AJ, in press

Steidel, C. C., & Hamilton, D. 1992, AJ, 104, 941

——— . 1993, AJ, 105, 2017

Steidel, C. C., Pettini, M., & Hamilton, D. 1995, AJ, 110, 2519

Storrie-Lombardi, L. J., McMahon, R. G., Irwin, M. J., & Hazard, C. 1994, ApJ, 427, L13

Sutherland, R. S., & Shull, J. M. 1996, in preparation

Thielemann, F. K., Nomoto, K., & Yokoi, K. 1986, A&A, 158, 17

Tinsley, B. M. 1980, Fund. Cosmic Phys., 5, 287

Tytler, D., Fan, X.-M., Burles, S., Cottrell, L., Davis, C., Kirkman, D., & Zuo, L. 1995, in QSO Absorption Lines, Proc. ESO Workshop, ed. G. Meylan (Heidelberg: Springer), 289

van den Bergh, S., Abraham, R. G., Ellis, R. S., Tanvir, N. R., Santiago, B. X., & Glazebrook, K. 1996, AJ, in press

van der Marel, R. P. 1991, MNRAS, 253, 710

Warren, S. J., Hewett, P. C., & Osmer, P. S. 1994, ApJ, 421, 412

White, S. D. M., & Frenk, C. S. 1991, ApJ, 379, 25

Williams, R. E., et al. 1996, AJ, in press

Woosley, S. E., & Weaver, T. A. 1995, ApJS, 101, 181

Yoshii, Y., & Peterson, B. 1994, ApJ, 436, 551

FIGURE CAPTIONS

Figure 1: (*a*) Mean cosmic transmission for a source at $z_{em} = 2.5, 3.5$, and 4.5 (*solid lines*), as a function of observed wavelength. The characteristic staircase profile is due to continuum blanketing from the Lyman series. Also plotted are the response functions of the four broad passbands, F300W (*dotted line*), F450W (*short-dashed line*), F606W (*long-dashed line*), and F814W (*dash-dotted line*) used for the *Hubble Deep Field*. (*b*) Magnitude increments ΔU_{300} (*dotted line*), ΔB_{450} (*short-dashed lines*), ΔV_{606} (*long-dashed line*), and ΔI_{814} (*dash-dotted line*), derived by integrating the mean cosmic transmission over the corresponding bandpass, as a function of the emission redshift.

Figure 2: (*a*) Apparent synthetic colors of a star-forming galaxy with constant SFR (age 0.3 Gyr) plotted as a function of the emission redshift. Each pair of curves depicts, from top to bottom, the attenuated colors and the colors observed in the case of negligible intergalactic absorption. *Solid lines: $U_{300} - B_{450}$. Dashed lines: $B_{450} - V_{606}$. Dotted lines: $V_{606} - I_{814}$.* (*b*) The colors of the four brightest starburst galaxies observed by *HUT* (see text for details). *Empty dots: $U_{300} - B_{450}$. Filled dots: $B_{450} - V_{606}$. Triangles: $V_{606} - I_{814}$.* All spectra have been reddened by intergalactic absorption.

Figure 3: $U_{300} - B_{450}$ vs. $B_{450} - V_{606}$ for model galaxies. A total of 103879 synthetic spectra of galaxies representing a wide range of ages, star formation histories, metallicities, dust contents, and redshifts, were folded through the HDF bandpasses. The galaxies shown as small points are at redshifts less than 2 or redshifts greater than 3.5. Galaxies shown as large solid circles are those in the redshift range $2 < z < 3.5$ with ages less than 10^8 yr and extinctions $A_B < 1$. Large x's are galaxies in the same redshift range that have ages greater than 10^8 yr or $A_B > 1$. Our color selection criteria are shown as the large polygon. Galaxies within the polygon in the HDF observations are selected as likely candidates for $2 < z < 3.5$ objects. The selection criteria are $U_{300} - B_{450} > 1.3$, $U_{300} - B_{450} > B_{450} - I_{814} + 1.2$, and $B_{450} - I_{814} < 1.5$.

Figure 4: Selection efficiency for F300W dropouts. This figure provides a measure of color selection in isolating galaxies with $2 < z < 3.5$. The solid histogram shows the fraction of models in each redshift interval ($\Delta z = 0.2$) that meet the color selection criteria. The dotted histogram shows the fraction of models with ages less than 10^8 yr and extinctions $A_B < 2$ that meet the selection criteria. The color selection criteria are extremely efficient at identifying relatively unobscured star-forming galaxies with $2 < z < 3.5$, and separating them from the chaff at other redshifts.

Figure 5: $B_{450} - V_{606}$ vs. $V_{606} - I_{814}$ for model galaxies. The galaxies shown as small points are at redshifts less than 3.5 or redshifts greater than 4.5. Galaxies shown as large solid circles are those in the redshift range $3.5 < z < 4.5$ with ages less than 10^8 yr and extinctions $A_B < 1$. Large x's are galaxies in the same redshift range that have ages greater than 10^8 yr or $A_B > 1$. Our color selection criteria are shown as the large polygon. Galaxies within the polygon in the HDF observations are selected as likely candidates for $3.5 < z < 4.5$ objects. The selection criteria are $B_{450} - V_{606} > 1.7(V_{606} - I_{814}) + 0.7$, $B_{450} - V_{606} > 1.5$, $B_{450} - V_{606} < 3.5(V_{606} - I_{814}) + 1.5$, and $V_{606} - I_{814} < 1.5$.

Figure 6: Selection efficiency for F450W dropouts. This figure provides a measure of color selection in isolating galaxies with $3.5 < z < 4.5$. The solid histogram shows the fraction of models in each redshift interval ($\Delta z = 0.2$) that meet the color selection criteria. The dotted histogram shows the fraction of models with ages less than 10^8 yr and extinctions $A_B < 2$ that meet the selection criteria. The primary source of contamination for the sample is galaxies at slightly lower redshifts with intrinsically red colors. The dashed line shows the fraction of the models with ages greater than 10^9 yr or $A_B > 2$ that meet the selection critera. If such red objects at $2 < z < 3.5$ are very common, then our derived metal formation rate at higher redshifts may be an overestimate. However, we suspect that such old or dusty interlopers are much less common than blue star-forming galaxies at slightly higher redshift.

Figure 7: $U_{300} - B_{450}$ vs. $B_{450} - I_{814}$ color-color plot of galaxies in the *Hubble Deep Field* satistying magnitude ranges given in the text. (*a*) Objects undetected in F300W (with signal-to-noise <1) are plotted

as triangles at the 1σ lower limits to their $U_{300} - B_{450}$ colors. Symbol size scales with the I_{814} magnitude of the object. The dashed lines outline the selection region within which we identify candidate $2 < z < 3.5$ objects. (*b*) Location in the color-color diagram of the more than 60 galaxies in the HDF which have known Keck/LRIS spectroscopic redshifts from Steidel et al. (1996b), Cohen et al. (1996), and Moustakas et al. (1996).

Figure 8: $B_{450} - V_{606}$ vs. $V_{606} - I_{814}$ color-color plot of galaxies in the *Hubble Deep Field* satistying magnitude ranges given in the text. (*a*) The symbol types and sizes are as described for Fig. 7*a*. The selection area we define for candidate $3.5 < z < 4.5$ galaxies is outlined with dashed lines. (*b*) Same as Fig. 7*b*.

Figure 9: Element and star formation history of the universe. The data points from various surveys provide a measurement or a lower limit to the universal metal ejection density, $\dot{\rho}_Z$, as a function of redshift. For a Salpeter IMF, to translate $\dot{\rho}_Z$ into a total star formation density, $\dot{\rho}_*$, a factor of 42 should be applied. *Triangle:* Gallego et al. (1995). *Filled dots:* Lilly et al. (1996). *Diagonal cross:* lower limit from Steidel et al. (1996a). *Filled squares:* lower limits from the *Hubble Deep Field* images. The dashed line depicts the fiducial rate, $\dot{\Sigma}_Z$, given by the mass density of metals observed today divided by the present age of the universe (see text for details). A flat cosmology with $q_0 = 0.5$ and $H_0 = 50 \, \mathrm{km \, s^{-1} \, Mpc^{-1}}$ has been assumed.
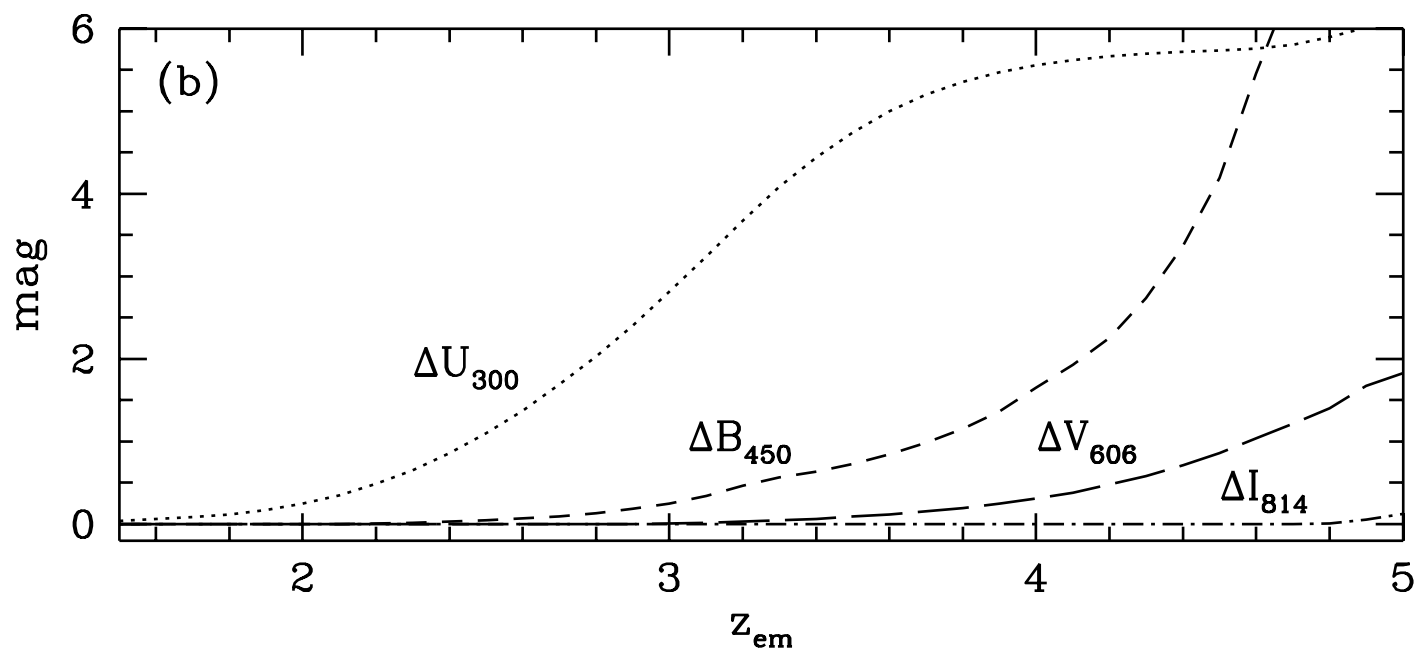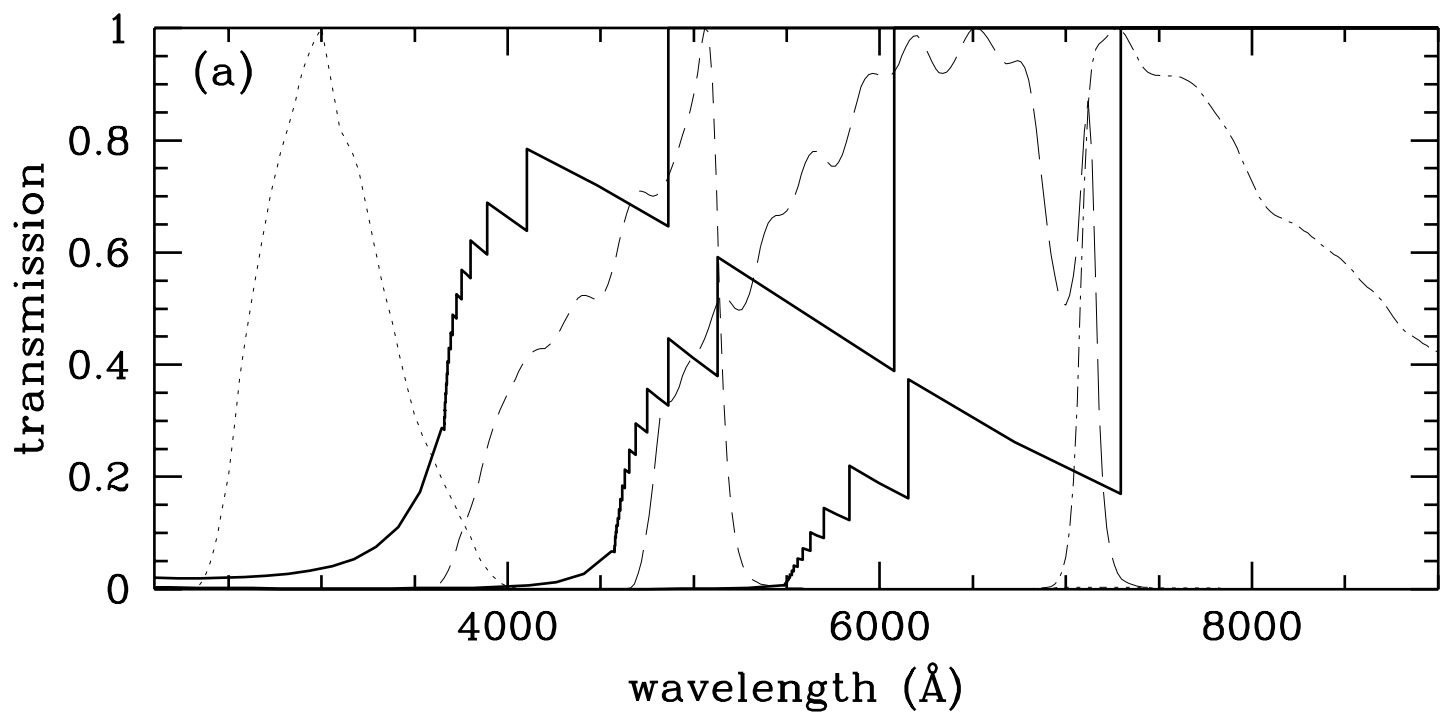
(a)

transmission

wavelength (Å)

(b)

mag

ΔU_{300}

ΔB_{450}

ΔV_{606}

ΔI_{814}

z_{em}

TABLE 1. Parameters Grid of Synthetic Spectra

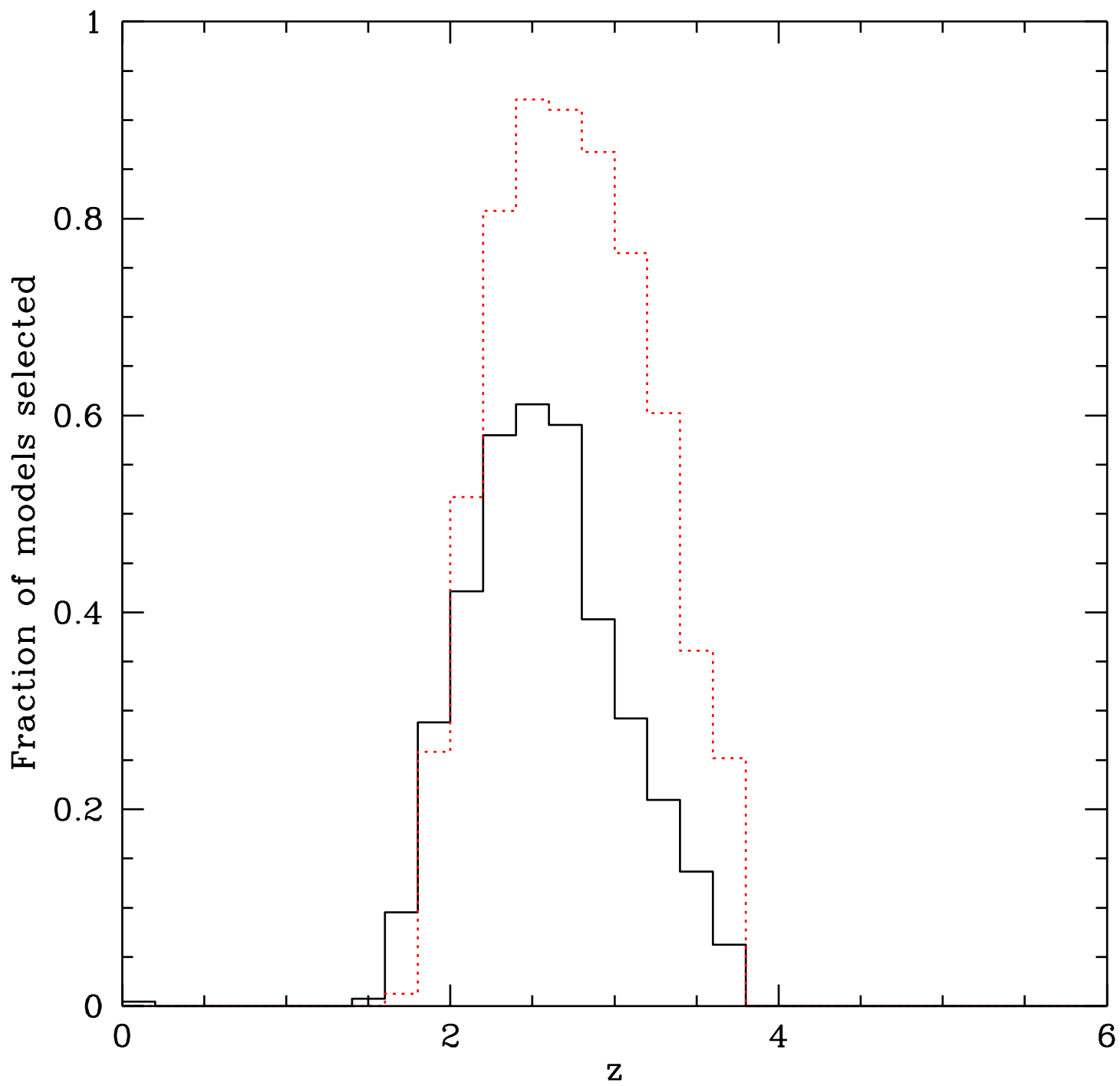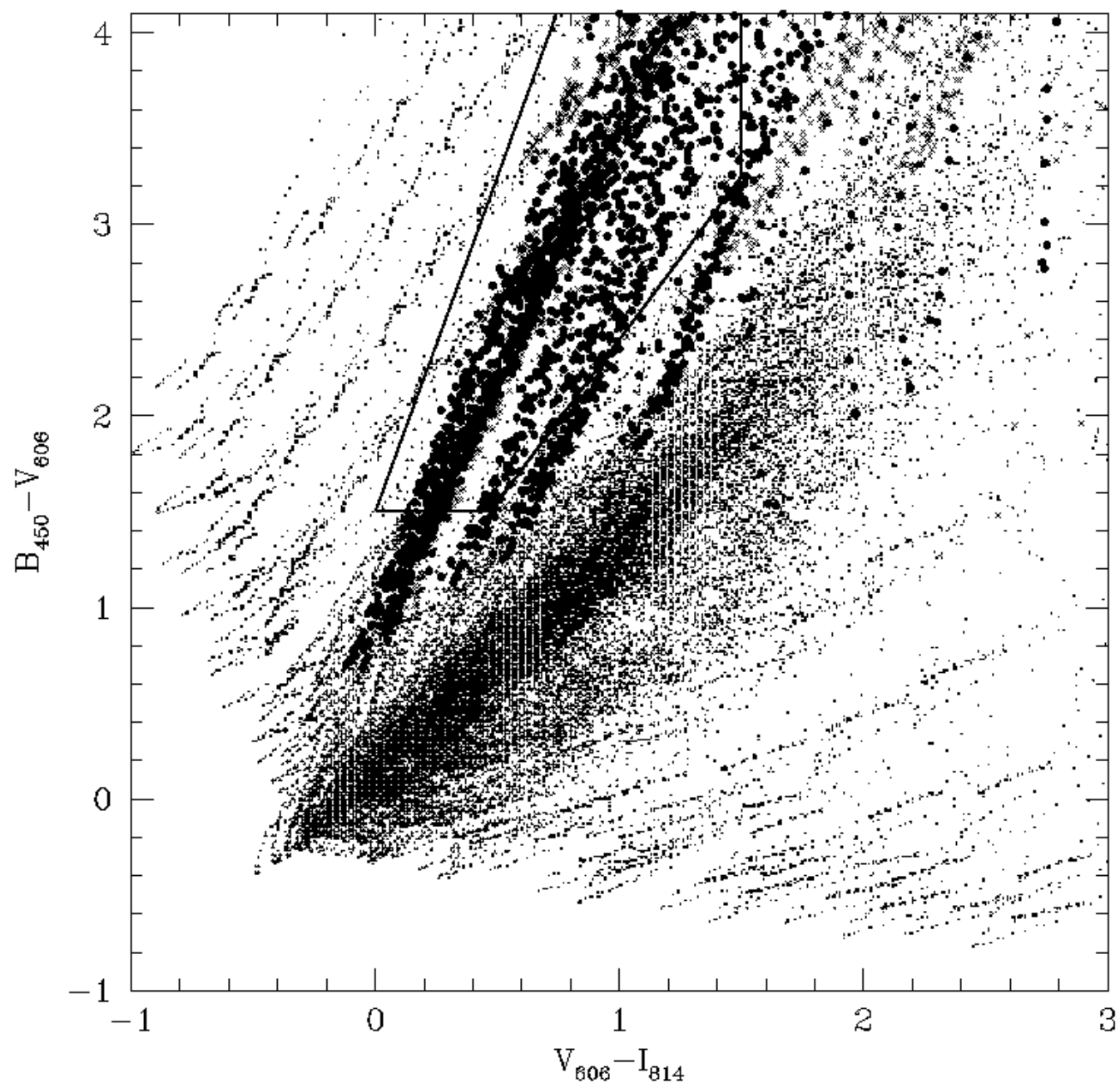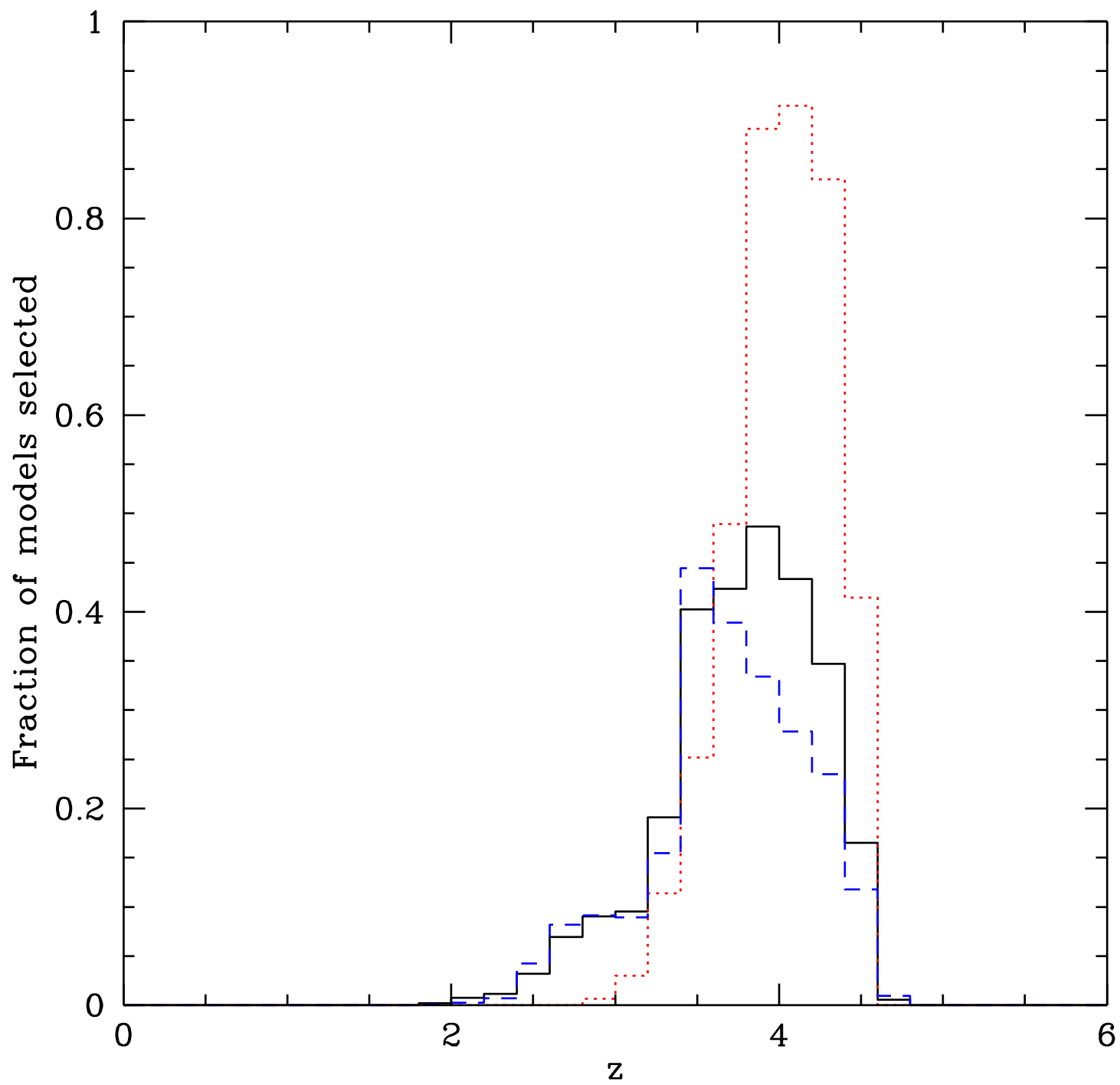|	
Exponental Star Formation Timescales	$10^7, 10^8, 10^9, 5 \times 10^9, 10^{10}, 3 \times 10^{10}$ yr
Constant Star Formation Durations	10^7 yr
Metallicities	$Z_\odot, Z_\odot/100$
A_B	0, 0.5, 1, 2, 3, 4, 5
Extinction Laws	Galactic, LMC, SMC
Redshifts	0.001 0.01 0.05 0.1 0.15 0.2 0.25 0.3 0.35
	0.4 0.45 0.5 0.55 0.6 0.64 0.7 0.75 0.8
	0.85 0.9 0.95 1.0 1.1 1.2 1.3 1.4 1.5
	1.6 1.7 1.8 1.9 2.0 2.1 2.2 2.3 2.4
	2.5 2.6 2.7 2.8 2.9 3.0 3.1 3.2 3.3
	3.4 3.5 3.6 3.7 3.8 3.9 4.0 4.1 4.2
	4.3 4.4 4.5 4.6 4.7 4.8 4.9 5.0 5.2
	5.4 5.6 5.8 6.0 6.2 6.4 6.6 6.8 7.0
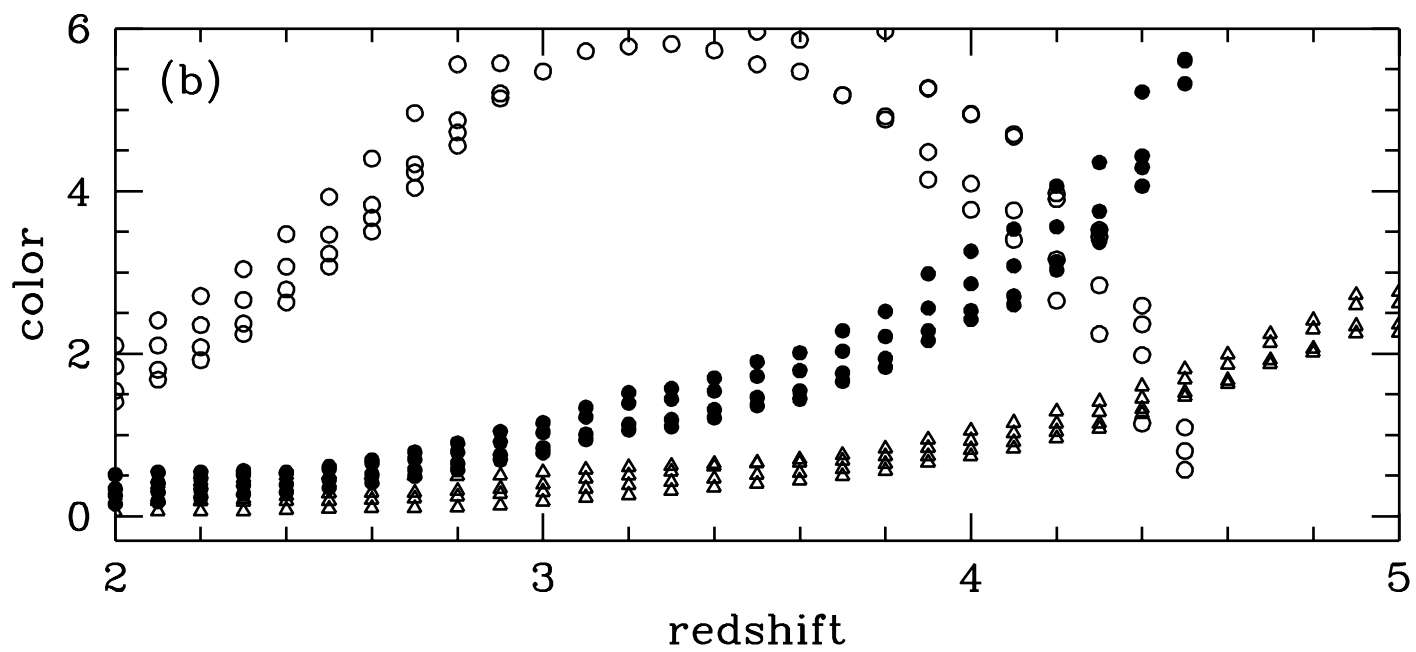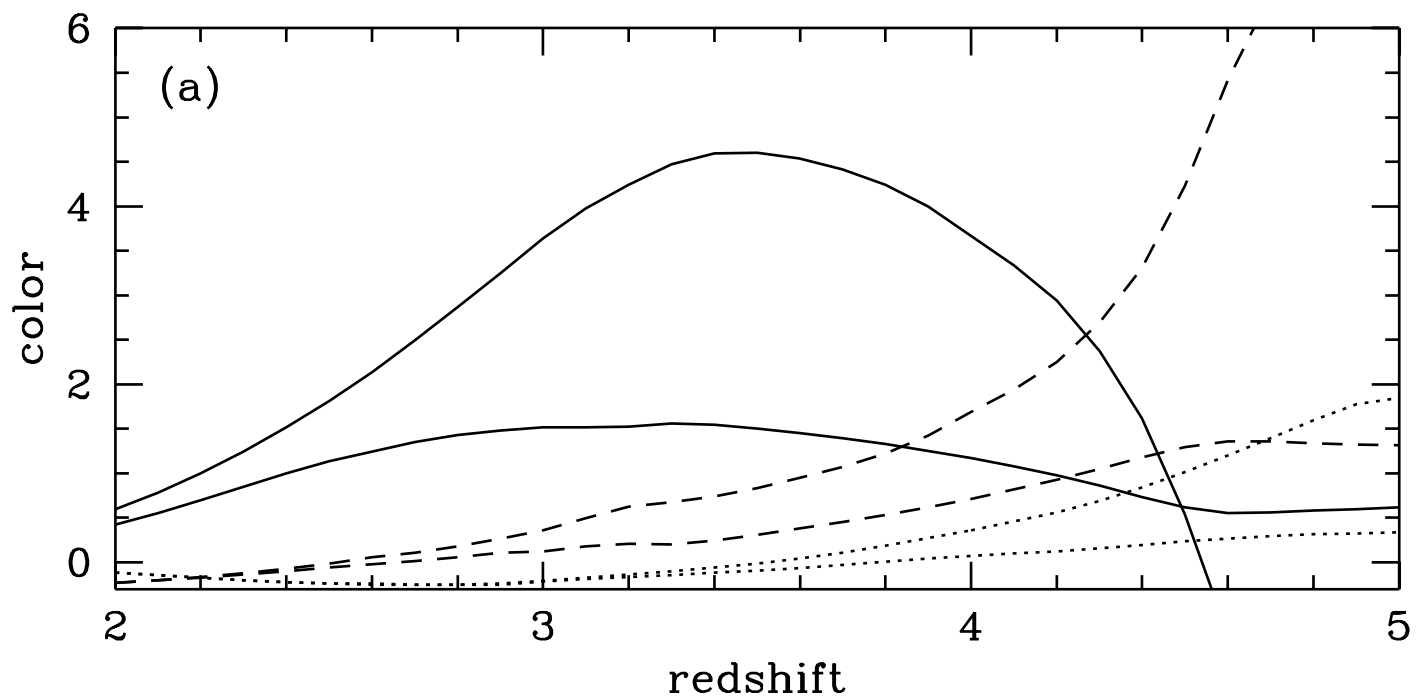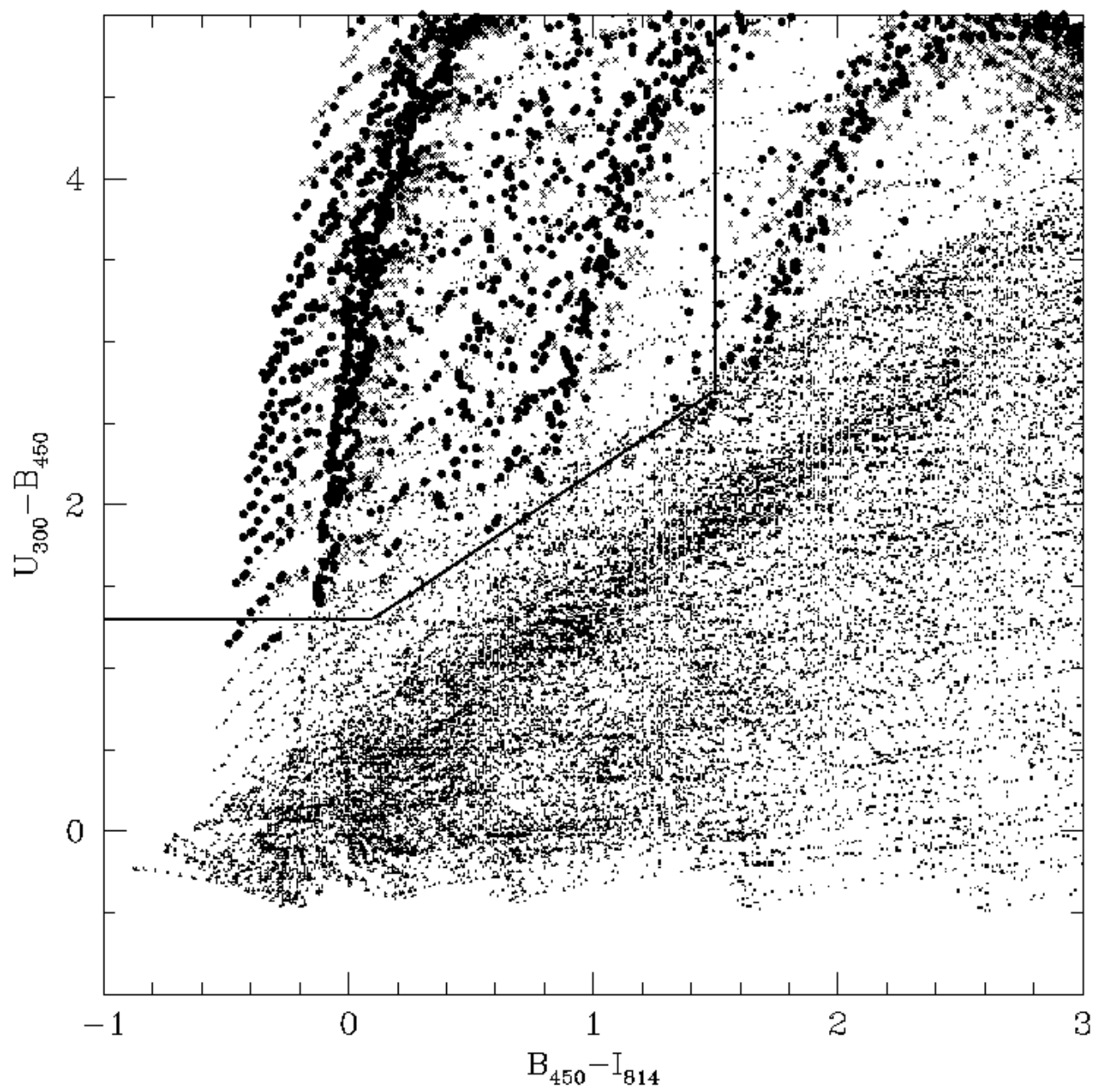
TABLE 2. HDF U_{300} Dropouts

ID	α (h:m:s)	δ (°:′:″)	U_{300}	B_{450}	V_{606}	I_{814}
2-82.1	12:36:43.977	62:14:10.95	26.62	24.77	24.72	24.74
2-122.0	12:36:47.677	62:13:19.99	>28.88	26.28	25.75	25.65
2-213.0	12:36:46.679	62:13:55.78	>28.64	26.67	26.21	26.10
2-392.0	12:36:49.724	62:13:44.05	28.55	26.54	26.44	26.44
2-456.12	12:36:49.840	62:13:50.41	>29.36	26.77	26.30	26.13
2-456.22	12:36:49.938	62:13:53.02	26.81	25.27	25.19	25.11
2-525.0	12:36:50.034	62:14:02.06	27.44	25.17	24.88	24.70
2-547.0	12:36:51.272	62:13:45.69	27.94	26.07	25.93	25.89
2-565.1	12:36:51.100	62:13:49.81	>29.54	26.66	25.99	25.72
2-637.0	12:36:52.670	62:13:40.11	>28.82	26.23	25.31	25.07
2-643.0	12:36:53.335	62:13:30.55	>28.50	25.71	24.89	24.62
2-726.0	12:36:53.035	62:13:47.28	>28.61	26.44	25.84	25.63
2-741.0	12:36:52.061	62:14:06.78	28.69	26.64	26.28	26.23
2-751.0	12:36:54.115	62:13:36.86	27.70	26.24	26.43	26.49
2-822.0	12:36:53.912	62:13:52.64	28.31	26.57	26.71	26.80
2-824.0	12:36:54.539	62:13:42.39	27.25	25.41	25.27	25.29
2-889.0	12:36:52.151	62:14:31.55	>28.53	26.36	25.84	25.69
2-890.0	12:36:51.986	62:14:34.87	28.30	26.02	25.94	25.80
2-903.0	12:36:54.988	62:13:48.03	26.72	24.79	24.62	24.57
2-949.0	12:36:54.511	62:14:04.70	27.80	25.96	25.66	25.58
2-999.0	12:36:56.545	62:13:40.81	>28.48	26.13	25.83	25.28
3-41.0	12:36:53.514	62:13:18.95	>29.03	26.09	26.06	26.08
3-83.0	12:36:56.709	62:13:25.13	27.62	25.90	25.69	25.56
3-221.2	12:36:57.778	62:13:16.31	>29.45	26.54	25.78	25.44
3-286.0	12:36:49.522	62:12:45.69	28.46	26.52	26.42	26.39
3-504.0	12:36:57.533	62:12:50.22	27.72	26.19	26.17	26.10
3-510.0	12:36:51.863	62:12:32.50	>28.61	26.53	26.22	26.12
3-550.0	12:36:51.246	62:12:28.54	26.45	24.94	24.87	24.85
3-677.0	12:36:51.531	62:12:18.34	28.37	25.90	25.55	25.14
3-736.0	12:36:55.547	62:12:24.67	27.89	26.37	26.38	26.36
3-748.0	12:36:59.889	62:12:36.98	>28.84	26.54	26.16	26.07
3-813.0	12:36:59.152	62:12:28.32	>28.78	26.58	25.86	25.78
3-902.0	12:36:51.698	62:11:58.84	>28.51	26.19	26.01	26.07
3-916.0	12:36:58.208	62:12:17.61	28.24	25.94	25.60	25.35
4-83.0	12:36:50.294	62:12:06.09	>28.87	26.77	26.21	26.07
4-85.2	12:36:49.593	62:12:20.67	28.08	25.55	25.31	25.22
4-96.0	12:36:47.821	62:12:44.15	28.76	26.65	26.65	26.67
4-194.0	12:36:49.707	62:11:56.45	>28.80	26.62	25.98	25.79
4-252.0	12:36:45.500	62:12:55.71	27.93	26.47	26.40	26.36
4-289.0	12:36:46.858	62:12:27.11	>28.69	25.45	25.20	25.22
4-316.0	12:36:44.997	62:12:51.84	26.01	24.42	24.28	24.13
4-317.0	12:36:48.661	62:11:48.68	>29.18	26.35	26.21	26.28
4-363.0	12:36:48.213	62:11:46.88	>28.37	25.91	25.22	25.05
4-389.0	12:36:45.537	62:12:25.93	>28.93	26.52	26.28	26.23
4-488.0	12:36:46.436	62:11:46.60	28.23	26.13	26.04	25.99
4-491.0	12:36:43.164	62:12:39.89	27.84	25.08	24.89	24.86
4-497.0	12:36:45.639	62:11:58.34	>28.93	26.11	25.83	25.75
4-555.1	12:36:45.320	62:11:54.20	27.48	24.26	23.57	23.33
4-588.0	12:36:41.790	62:12:44.69	>28.07	25.99	25.43	25.31
4-590.0	12:36:43.221	62:12:19.30	28.56	26.29	26.02	25.80
4-599.0	12:36:43.104	62:12:20.21	28.57	26.57	26.28	26.29
4-639.1	12:36:41.623	62:12:39.78	>28.48	24.91	24.82	24.65
4-660.0	12:36:42.861	62:12:12.56	28.60	25.98	25.93	25.95
4-676.0	12:36:41.619	62:12:32.07	>28.47	25.70	25.47	25.42
4-681.0	12:36:44.511	62:11:40.47	29.02	26.55	26.50	26.57
4-825.0	12:36:42.236	62:11:51.38	27.75	26.34	26.38	26.30
4-926.2	12:36:39.473	62:12:14.86	>29.06	26.41	25.57	25.42
4-936.0	12:36:40.712	62:11:51.63	29.07	26.73	26.67	26.67

TABLE 3. HDF B_{450} Dropouts

ID	α (h:m:s)	δ (°:′:″)	U_{300}	B_{450}	V_{606}	I_{814}
2-493.0	12:36:50.552	62:13:50.39	>29.19	29.15	27.57	27.47
2-977.0	12:36:55.682	62:13:51.95	>29.01	28.45	26.70	26.25
3-195.0	12:36:48.488	62:12:49.54	28.05	28.17	26.39	25.98
3-223.0	12:36:52.697	62:12:59.98	29.06	29.59	27.44	26.80
3-231.1	12:36:51.825	62:12:56.72	>29.20	>29.95	27.53	26.60
3-512.0	12:36:56.031	62:12:45.71	>28.50	27.58	25.91	25.56
3-534.2	12:36:59.156	62:12:55.41	>29.60	29.76	27.61	26.80
3-675.0	12:36:57.085	62:12:35.33	>28.67	27.76	26.16	25.70
3-705.0	12:36:51.601	62:12:16.12	>29.05	28.86	26.98	26.66
3-783.0	12:36:58.865	62:12:30.05	28.87	29.62	27.12	26.28
4-277.0	12:36:48.854	62:11:53.88	>29.19	29.75	27.24	26.18
4-280.0	12:36:46.583	62:12:31.15	29.03	29.25	27.17	26.88
4-439.0	12:36:43.753	62:12:42.63	>28.63	>29.39	26.06	24.97
4-702.0	12:36:43.540	62:11:51.82	28.51	>29.81	27.53	26.65

HDF WF1-3

$I_{814} = 26$

HDF WF1-3

HDF WF1-3

$B_{450} - V_{606}$

$V_{606} - I_{814}$

$\bigcirc \triangle \quad I_{814} = 26$

HDF WF1-3